Graph Distribution-valued Signals in Wasserstein Spaces: Theory and Applications

Yanan Zhao, Feng Ji, Xingchao Jian and Wee Peng Tay, *Senior Member, IEEE*

arXiv:2607.20008v1 [eess.SP] 22 Jul 2026

***Abstract*—We introduce a framework for graph signal processing (GSP) in which signals are represented as graph distribution-valued signals (GDSs), i.e., probability measures in a Wasserstein space. This perspective addresses fundamental limitations of classical vector-based GSP, including the requirement for complete synchronous observations across vertices and the need for strict temporal correspondence in observed filter input–output pairs. Furthermore, by modeling the graph structure as a distribution conditioned on signal realizations, we provide a principled approach to signal-dependent graph structures, which are common in real-world applications, while explicitly encoding uncertainty in graph topology. Our framework inherently captures uncertainty and stochasticity while strictly generalizing traditional graph signals, which can be interpreted as Dirac delta measures. We develop a systematic correspondence between foundational GSP concepts and their GDS analogs, showing that classical formulations emerge as special cases of our framework. We establish theoretical continuity results for GDS transforms, providing stability guarantees for input perturbations and distribution approximations. We demonstrate the utility of this approach through example applications, including graph filter learning and anomaly detection, and validate its effectiveness through empirical studies.**

***Index Terms*—Graph distribution-valued signals, graph signal processing, Wasserstein spaces**

I. Introduction

Graphs provide a powerful framework for modeling complex systems in diverse domains, including social networks, transportation systems, and sensor networks. In the classical graph signal processing (GSP) framework [1]–[6], graph signals are represented as vectors, where each entry corresponds to the value at a specific node. This representation enables the application of linear operators such as the graph Fourier transform (GFT), convolution, and graph filters [2], [3], [7] to analyze signal structure and inter-node relationships.

Despite its widespread adoption, the vector-based GSP framework exhibits several critical limitations: (i) *Assumption of complete observations;* Classical GSP frameworks assume that signals are observed synchronously and completely across all nodes, so that operators such as the GFT can be applied to the full signal vector. However, in practice, data collection is often asynchronous or incomplete [5], [8], [9], making this assumption unrealistic. (ii) *Requirement for strict signal correspondence.* While statistical GSP methods [10]–[15] incorporate randomness via random variables, graph filters are still defined as vector-to-vector mappings and require paired input–output signals, e.g., $\{(\mathbf{x}_i, \mathbf{y}_i)\}_{i=1}^m$, with the filter $\mathbf{F}$ trained to satisfy $\mathbf{F}(\mathbf{x}_i) \approx \mathbf{y}_i$. This imposes a rigid one-to-one correspondence between input and output signals. In practice, such alignment is often imperfect due to temporal shifts, overlaps, periodic patterns, or missing and shuffled data, thereby limiting the applicability of these methods. (iii) *Assumption of a deterministic graph topology.* Classical GSP represents graph signals as vectors indexed by the vertices of a *fixed* graph, and defines the GFT via the eigendecomposition of a predetermined graph shift operator (GSO) (e.g., the adjacency matrix, Laplacian matrix, or their normalized variants). This formulation inherently assumes that the graph topology is fully known and deterministic. In many applications, however, the graph structure may be uncertain or partially observed [16]–[19], posing significant challenges to this classical framework.

To address these challenges, we model both graph signals and graph topologies as probability distributions rather than as random vectors or sample realizations. In contrast to statistical GSP, which typically operates either on samples with prior information like stationarity [10], [11], [13], [15], our framework treats the full probability distribution as the fundamental signal object. Accordingly, filters are optimized directly in distribution space, rather than in the node-value vector space. When the signal and topology distributions are unknown, they are first estimated from samples, and these estimates are then used for filter learning. This differs from statistical GSP, where filters are learned directly from samples. Most statistical GSP methods therefore remain subject to the limitations discussed above, because they continue to rely on vector-based signal representations. In our framework, the classical vector space of graph signals is replaced by the Wasserstein space [20]–[22], whose elements are probability measures on $\mathbb{R}^N$; we call such a signal a **graph distribution-valued signal (GDS)**. As a further generalization, we model the graph structure itself as a distribution conditioned on the signal realization, referred to as **signal adaptive graph structure (SAGS)**.

To illustrate the distinction from statistical GSP, consider COVID-19 daily case counts from 58 counties (2020–2022). In classical statistical GSP, each day is represented as a graph signal vector $\mathbf{x} \in \mathbb{R}^{58}$, where the i-th entry is the reported count in county i. This representation is convenient when county-level records are complete. In practice, however, many days include missing county reports. The vector-based approach then requires either discarding incomplete days, which can cause substantial data loss, or imputing missing values, which may introduce bias into subsequent filter learning. In contrast, the GDS framework treats county-level observations over time as samples from an underlying joint *probability distribution*, rather

The authors are with the School of Electrical and Electronic Engineering, Nanyang Technological University, 639798, Singapore. (e-mail: yanan002, jifeng, xingchao001, wptay@ntu.edu.sg).

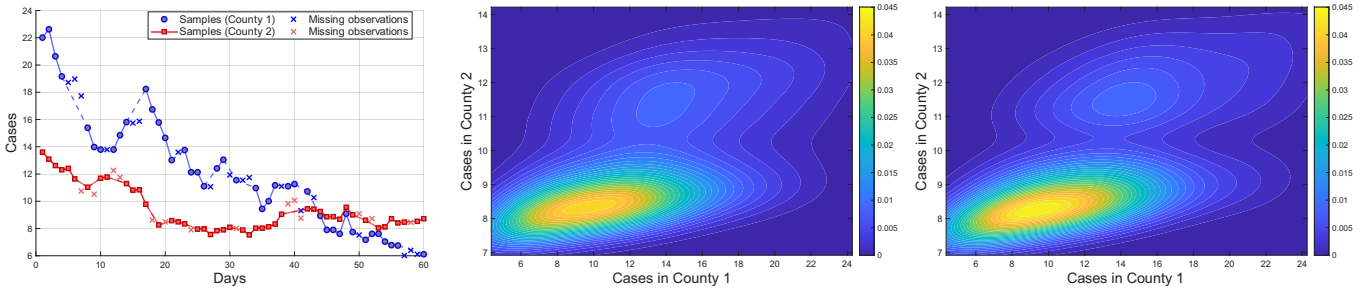

(a) Daily cases from two counties (b) Joint distribution from complete observations (c) Joint distribution from partial observations

Fig. 1. (a) COVID-19 daily cases from two counties over 60 days, together with the corresponding partial observations generated using an independent per-county missing rate of 20%; crosses indicate the masked entries. (b) Joint distribution estimated from the complete observations using KDE-estimated marginals and a Gaussian copula, representing the fully observed trajectories in (a) as realizations from an underlying distribution within the GDS framework. (c) Joint distribution estimated from the partial observations using the same Gaussian-copula model.

than as isolated daily vectors. Filtering is thus learned in the Wasserstein space of probability measures instead of the vector space of node-valued graph signals. This perspective captures both day-to-day variability and inter-county dependence.

Fig. 1 illustrates this distinction: Fig. 1a shows 60 days of two-county case counts as vector-valued samples, whereas Fig. 1b shows the corresponding joint distribution estimated from the same period using KDE marginals and a Gaussian copula. Under missing observations, this formulation can still leverage partial data through distribution estimation rather than requiring complete daily vectors. For an independent per-county missing rate of 20%, the probability that a two-dimensional daily observation is complete is 0.64; hence only about 38 of 60 days are directly usable as complete vectors. By contrast, each county retains about 80% of its observations for marginal estimation, while pairwise-complete observations are used to estimate copula dependence. As shown in Figs. 1b and 1c, the Gaussian-copula estimate from partial observations remains close to the complete-observation estimate. Their discrepancy is quantified by

$$d_{\mathrm{TV}}\left(\hat{\mu}_{\mathrm{full}}, \hat{\mu}_{\mathrm{partial}}\right) = \frac{1}{2}\int_{\mathbb{R}^2} \left|\hat{p}_{\mathrm{full}}(\mathbf{x}) - \hat{p}_{\mathrm{partial}}(\mathbf{x})\right| \, \mathrm{d}\mathbf{x},$$

where $\hat{p}_{\mathrm{full}}$ and $\hat{p}_{\mathrm{partial}}$ denote densities estimated from complete and partial observations, respectively. The resulting value, $d_{\mathrm{TV}} = 0.043$, indicates that the dominant distributional structure is preserved despite missing entries. The effect of missing observations is further examined in Section V-A and Fig. 3a, where we compare vector-based GSP filtering with the proposed GDS framework.

This flexibility comes with a trade-off. Classical statistical GSP is simpler when complete, reliable vector-valued samples are available. The GDS framework instead requires estimation of the underlying joint distribution, including inter-county dependence, so its performance depends on distribution-model quality. Nevertheless, when missingness, sampling variability, and spatial dependence are substantial, learning filters in distribution space provides a more flexible alternative to vector-based statistical GSP.

Our framework is a generalization of classical GSP by replacing the underlying vector space with the Wasserstein space, so that traditional graph signals, which correspond to Dirac delta distributions, become special cases of GDSs. This generalization enables a principled treatment of uncertainty and facilitates richer modeling of graph-structured data. Beyond generalizing the signals, we also substitute fixed graph topology with signal-adaptive graph structures, yielding a flexible framework that accommodates uncertainty in both signals and graphs. Methodologically, this shift requires moving away from linear algebra toward tools from analysis and probability theory, giving our approach the flavor of classical Fourier theory [23] rather than that of algebraic signal processing [24].

While this greater flexibility brings clear modeling benefits, it also introduces practical challenges. For example, the GDS framework requires additional data to accurately estimate distributions, especially in high-dimensional settings. In practice, applications often do not require full distributional knowledge. Instead, one can assume a parametric model like a Gaussian copula to capture key statistical properties. In some other applications like node classification, deep learning models can be employed to learn a proxy distribution given by the softmax output of the model for the node labels, with the GDS framework applied to filter these node distributions for downstream tasks [25], [26]. Another challenge is increased computational complexity due to operations in the Wasserstein space. However, this can be mitigated by working with tractable families of distributions, as justified by our theory and demonstrated in our numerical experiments (cf. Section V).

Our main contributions are summarized as follows:

- We develop a unified GDS framework and its generalized extension in which graph signals are modeled as probability measures in Wasserstein space and graph topologies are modeled as signal-adaptive distributions. Within this framework, we define distribution-level analogs of core GSP operations (Fourier transform, filtering, and convolution) and provide a systematic dictionary from classical GSP to GDS, with vector-valued GSP recovered as a special case.
- We establish new analytic guarantees for generalized GDS transforms, including uniform continuity on compact signal domains and pointwise continuity under a Lipschitz

condition on the induced transform distribution. These results provide a stability foundation for learning and inference from approximate distributions and perturbed inputs.
- We illustrate the GDS framework in two representative tasks, graph filter learning and anomaly detection, and verify through numerical experiments that the distribution-level formulation is practically effective, particularly under incomplete or misaligned observations.

This paper builds on our preliminary work in [27], which introduced the GDS representation of graph signals as probability measures in Wasserstein space. In this extended version, we (i) generalize from fixed graph structure to signal-adaptive random graph structure, (ii) formalize a systematic operator-level correspondence between GSP and GDS, (iii) establish continuity-based stability theory for generalized transforms, and (iv) demonstrate concrete gains in graph filter learning and anomaly detection. These additions address the main limitations of the preliminary version, namely limited formal development and lack of application-level validation.

Because the signals of interest in this work are probability distributions in Wasserstein spaces, we formulate the GDS framework in terms of probability measures rather than random variables. To facilitate comparison with classical GSP, whenever a main GDS-related definition involves a probability distribution μ, we accompany it with *the statement* "$\triangleright\ \mathbf{x} \sim \mu$", indicating the random variable $\mathbf{x}$ distributed according to μ.

The rest of this paper is organized as follows. Section II formulates the mathematical setting underlying our theory via the Wasserstein space. The complete GDS framework is then developed in Section III and Section IV. Example applications of the GDS framework are presented in Section III-C and Section IV-D, and numerical results in Section V, followed by concluding remarks in Section VI.

Notation. Scalars and scalar-valued functions are denoted by plain lowercase letters (e.g., x), whereas vectors and vector-valued functions are denoted by bold lowercase letters (e.g., $\mathbf{x}$). Matrices are denoted by bold uppercase letters (e.g., $\mathbf{A}$), and linear operators are also written in boldface. Probability distributions are denoted by lowercase Greek letters (e.g., μ, ν, γ), with δ reserved for the Dirac measure. Calligraphic letters denote spaces (e.g., $\mathcal{P}$), and G denotes a graph throughout. The set of real numbers is denoted by $\mathbb{R}$, and $M_N(\mathbb{R})$ denotes the space of $N \times N$ real matrices. The transpose is denoted by $(\cdot)^\intercal$, $\mathrm{Tr}(\cdot)$ denotes the trace operator, and $\|\cdot\|_{\mathrm{op}}$ denotes the operator norm induced by the Euclidean norm. The symbol $\circ$ denotes function composition. The pushforward of a measure μ through a function or operator $\mathbf{F}$ is denoted by $(\mathbf{F})_*\mu$. Throughout this paper, all measures are Borel measures.

II. Preliminaries: Wasserstein Spaces And Graph Distribution-Valued Signals

In this section, we first define the Wasserstein space and then introduce the notion of GDSs as probability measures in Wasserstein space, which generalizes traditional graph signals. We provide examples to illustrate the concept and underlying intuition.

Throughout this paper, we consider a connected, simple, and undirected graph $G = (V, \mathbf{A})$ with $|V| = N$ vertices and (weighted) edges represented by the adjacency matrix $\mathbf{A} = [a_{ij}]_{i,j\in\mathcal{V}}$. Its Laplacian is $\mathbf{L}_G = \mathbf{D} - \mathbf{A}$, where $\mathbf{D}$ is the degree matrix. We denote by $\mathbf{S}_G$ a generic graph shift operator, such as $\mathbf{A}$ or $\mathbf{L}_G$.

Recall that a traditional graph signal is a vector $\mathbf{x} \in \mathbb{R}^N$ that assigns a real value to each vertex. From a probabilistic perspective, this can be viewed as the Dirac measure $\delta_{\mathbf{x}}$. This motivates a natural generalization in which graph signals are modeled as probability measures on $\mathbb{R}^N$, residing in the Wasserstein space [20]. This probabilistic formulation unifies deterministic signals and their statistical descriptions, providing a foundation for the proposed GDS framework.

Definition 1 (Wasserstein space)**.** *Let $(\mathcal{X}, \|\cdot\|)$ be a normed space and $\mathcal{P}(\mathcal{X})$ the set of Borel probability measures on $\mathcal{X}$, i.e., $\mathcal{P}(\mathcal{X}) := \{\mu : \mu$ is a probability measure on $(\mathcal{X}, \mathcal{B}(\mathcal{X}))\}$, where $\mathcal{B}(\mathcal{X})$ is the Borel σ-algebra. For $p \geq 1$, the Wasserstein space of order p is*

$$\mathcal{P}_p(\mathcal{X}) = \left\{\mu \in \mathcal{P}(\mathcal{X}) : \int_{\mathcal{X}} \|\mathbf{x}\|^p \,\mathrm{d}\mu(\mathbf{x}) < \infty\right\}. \quad (1)$$

This space is equipped with the p-Wassertain distance: for $\mu_1, \mu_2 \in \mathcal{P}_p(\mathcal{X})$,

$$W_p(\mu_1, \mu_2) := \left(\inf_{\gamma\in\Gamma(\mu_1,\mu_2)} \int_{\mathcal{X}\times\mathcal{X}} \|\mathbf{x} - \mathbf{y}\|^p \,\mathrm{d}\gamma(\mathbf{x}, \mathbf{y})\right)^{1/p}, \quad (2)$$

where $\mu_1, \mu_2 \in \mathcal{P}_p(\mathcal{X})$, and $\Gamma(\mu_1, \mu_2)$ denotes the set of all couplings of μ_1 and μ_2, i.e., joint probability measures on $\mathcal{X} \times \mathcal{X}$ with marginals μ_1 and μ_2.

For a graph G, the node signal sample space is $\mathcal{X} = \mathbb{R}^N$ equipped with the Euclidean norm $\|\mathbf{x}-\mathbf{y}\|_2$. The corresponding Wasserstein space $\mathcal{P}_p(\mathbb{R}^N)$ consists of all probability measures on $\mathbb{R}^N$ with finite p-th moments.

Definition 2 (Graph distribution-valued signal)**.** *A graph distribution-valued signal (GDS) is a Borel probability measure $\mu \in \mathcal{P}_p(\mathbb{R}^N)$. The space $\mathcal{P}_p(\mathbb{R}^N)$ is referred to as the space of GDSs.*

The Wasserstein distance measures the minimal "work" required to transport one probability distribution to another, where work is the product of the mass and distance transported. Equipped with W_p, the space $\mathcal{P}_p(\mathbb{R}^N)$ is complete and separable [20]. While computing W_p for general measures is challenging, closed-form solutions exist in special cases.

Example 1. *(a) If $\mu_1 = \delta_{\mathbf{x}}$ and $\mu_2 = \delta_{\mathbf{y}}$, then $W_2(\delta_{\mathbf{x}}, \delta_{\mathbf{y}}) = d(\mathbf{x}, \mathbf{y})$. Thus, the space of traditional graph signals $\mathbb{R}^N$ embeds isometrically into the space of GDSs $\mathcal{P}_2(\mathbb{R}^N)$.*

(b) Let $\mu_1 = \mathcal{N}(\boldsymbol{m}_1, \boldsymbol{\Sigma}_1)$ and $\mu_2 = \mathcal{N}(\boldsymbol{m}_2, \boldsymbol{\Sigma}_2)$ be two non-degenerate Gaussian distributions on $\mathbb{R}^N$ with means $\boldsymbol{m}_1, \boldsymbol{m}_2$ and covariance matrices $\boldsymbol{\Sigma}_1, \boldsymbol{\Sigma}_2$ respectively. Then, their 2-Wasserstein distance is given by

$$W_2(\mu_1, \mu_2)^2 = \|\boldsymbol{m}_1 - \boldsymbol{m}_2\|_2^2 + \mathrm{Tr}\left(\boldsymbol{\Sigma}_1 + \boldsymbol{\Sigma}_2 - 2\left(\boldsymbol{\Sigma}_2^{1/2}\boldsymbol{\Sigma}_1\boldsymbol{\Sigma}_2^{1/2}\right)^{1/2}\right). \quad (3)$$

Therefore, minimizing the discrepancy between two Gaussian distributions in the Wasserstein space involves matching not only their means but also their covariances.

(c) Let $\mathrm{GMM}_K(\mathbb{R}^N)$ *denote the set of Gaussian mixture models (GMMs) on* $\mathbb{R}^N$ *with at most* K *components; i.e., the set of measures that can be written as* $\mu = \sum_{k=1}^{K'} a_k \mu_k$*, where* $K' \leq K$*,* $\mathbf{a} = (a_1, a_2, \ldots, a_{K'})^\intercal$*, and* $\{\mu_k\}_k$ *is a family of pairwise distinct Gaussian distributions (each with mean* $\mathbf{m}_k$ *and covariance matrix* $\mathbf{\Sigma}_k$*). Let* $\mathrm{GMM}_\infty(\mathbb{R}^N)$ *denote the set of all finite Gaussian mixtures on* $\mathbb{R}^N$*, i.e.,* $\mathrm{GMM}_\infty(\mathbb{R}^N) = \bigcup_{K\geq 0} \mathrm{GMM}_K(\mathbb{R}^N)$*. If* $\mu \in \mathrm{GMM}_K(\mathbb{R}^N)$ *and* $\nu \in \mathrm{GMM}_L(\mathbb{R}^N)$*, the Mixture-Wasserstein distance of order 2 [28] is defined as*

$$MW_2(\mu,\nu)^2 = \inf_{\gamma\in\Gamma(\mu,\nu)\cap \mathrm{GMM}_\infty(\mathbb{R}^{2N})} \int_{\mathbb{R}^N\times\mathbb{R}^N} \|\mathbf{x}-\mathbf{y}\|_2^2 \,\mathrm{d}\gamma(\mathbf{x},\mathbf{y}),$$

which admits the equivalent formulation [29]:

$$MW_2(\mu,\nu)^2 = \inf_{\omega\in\Pi(\mathbf{a},\mathbf{b})} \sum_{k,l} \omega_{kl} W_2(\mu_k,\nu_l)^2. \quad (4)$$

where $\mathbf{a} = (a_1, a_2, \ldots, a_K)^\intercal$ *and* $\mathbf{b} = (b_1, b_2, \ldots, b_L)^\intercal$ *are the mixture weights, and* $\Pi(\mathbf{a},\mathbf{b})$ *denotes the set of admissible couplings. Since the admissible couplings in* MW_2 *form a strict subset of those in* W_2*, this metric generally upper-bounds the classical Wasserstein distance; namely,* $MW_2(\mu,\nu) \geq W_2(\mu,\nu)$*. In practice,* $MW_2(\mu,\nu)$ *is often more tractable and can serve as a proxy for* $W_2(\mu,\nu)$ *in optimization problems.*

III. The GDS Processing Framework

In this section, we introduce a signal processing framework for GDSs that generalizes classical GSP. We first consider the basic setting in which the graph topology is fixed, and extend core GSP concepts to their GDS counterparts. To demonstrate the utility of the framework, we present an example application in graph filter learning. In Section IV, we further generalize the framework by allowing the graph distribution to be signal-adaptive.

A. GDS Fourier Transform

Recall that in traditional GSP, given a GSO $\mathbf{S}_G = \mathbf{U}_G\mathbf{\Lambda}_G\mathbf{U}_G^\intercal$, where $\mathbf{U}_G$ is the unitary matrix of eigenvectors and $\mathbf{\Lambda}_G$ is the diagonal matrix of eigenvalues, the GFT of a graph signal $\mathbf{x}\in\mathbb{R}^N$ is given by the orthogonal basis change $\widehat{\mathbf{x}} = \mathbf{U}_G^\intercal\mathbf{x}$. We extend this notion to GDSs as follows.

Definition 3 (GDS Fourier transform)**.** *Let* $\mathbf{S}_G = \mathbf{U}_G\mathbf{\Lambda}_G\mathbf{U}_G^\intercal$ *be a GSO, and let* $\mu\in\mathcal{P}_p(\mathbb{R}^N)$ *be a GDS on* G*. The* GDS Fourier transform (GDS-FT) *is the pushforward measure*

$$\hat{\mu} := (\mathbf{U}_G^\intercal)_*\,\mu \in \mathcal{P}_p(\mathbb{R}^N), \quad (5)$$

i.e., for any Borel set B*,* $\widehat{\mu}(B) = \mu\Big((\mathbf{U}_G^\intercal)^{-1}(B)\Big)$*. As a reminder, the symbol* $\triangleright$ *introduces the corresponding random variable interpretation:* $\triangleright\ \mathbf{x}\sim\mu,\ \mathbf{U}_G^\intercal\mathbf{x}\sim\hat{\mu}$*, which establishes the correspondence between classical GSP and our framework.*

Intuitively, GDS-FT transports a distribution from the vertex domain to the graph frequency domain via the pushforward induced by $\mathbf{U}_G^\intercal$. When $\mu = \delta_{\mathbf{x}}$ is a Dirac measure, we have $\widehat{\mu} = \delta_{\mathbf{U}_G^\intercal\mathbf{x}}$, which recovers the classical GFT. We have the following properties.

Proposition 1. *Let* G *be fixed graph with shift operator* $\mathbf{S}_G$ *and eigenbasis* $\mathbf{U}_G$*. Then the following properties hold.*

(i) (Well-definedness). The GDS-FT is well-defined, i.e., for any $\mu\in\mathcal{P}_p(\mathbb{R}^N)$*, we have* $\hat{\mu}\in\mathcal{P}_p(\mathbb{R}^N)$*.*

(ii) (Isometry). The GDS-FT is an isometry with respect to $W_p(\cdot,\cdot)$*, i.e., for* $\mu,\nu\in\mathcal{P}_p(\mathbb{R}^N)$*,*

$$W_p\left((\mathbf{U}_G^\intercal)_*\mu, (\mathbf{U}_G^\intercal)_*\nu\right) = W_p(\mu,\nu).$$

(iii) (Invertibility). The GDS-FT is invertible, with inverse given by $\mu = (\mathbf{U}_G)_*\widehat{\mu}$*.*

(iv) (Associativity). For $\mathbf{F}_G$ *and* $\mathbf{H}_G$*, we have*

$$(\mathbf{F}_G)_*\left((\mathbf{H}_G)_*\mu\right) = (\mathbf{F}_G\mathbf{H}_G)_*\mu.$$

(v) (Lipschitz stability under linear pushforward). For any linear map $\mathbf{A}\in\mathbb{R}^{N\times N}$*, the corresponding pushforward operator is Lipschitz continuous with respect to* $W_p(\cdot,\cdot)$*, i.e., for* $\mu,\nu\in\mathcal{P}_p(\mathbb{R}^N)$*,*

$$W_p((\mathbf{A})_*\mu, (\mathbf{A})_*\nu) \leq \|\mathbf{A}\|_{\mathrm{op}} W_p(\mu,\nu). \quad (6)$$

Proof: See Section A in the Appendix. ∎

Property (ii) states that the GDS-FT preserves the Wasserstein distance between distributions, serving as the distributional counterpart of the Parseval identity.

B. GDS Convolutional Filter

In classical GSP, a graph convolutional filter applies a linear transformation that selectively amplifies or suppresses certain frequency components of a graph signal. We now define the GDS version as follows.

Definition 4 (GDS convolutional filter)**.** *Let* $\mathbf{F}_G : \mathbb{R}^N \to \mathbb{R}^N$ *be a traditional graph convolutional filter. The* GDS convolutional filter *is the pushforward map*

$$\mathcal{F}_G : \mathcal{P}_p(\mathbb{R}^N) \to \mathcal{P}_p(\mathbb{R}^N), \quad \mu \mapsto (\mathbf{F}_G)_*\mu. \quad (7)$$

$\triangleright\ \mathbf{x}\sim\mu,\ \mathbf{F}_G\mathbf{x}\sim\mathcal{F}_G(\mu)$

When $\mu = \delta_{\mathbf{x}}$ is a Dirac measure at a single signal $\mathbf{x}$, we have $\mathcal{F}_G(\mu) = \delta_{\mathbf{F}_G\mathbf{x}}$, thereby recovering the classical graph convolution $\mathbf{F}_G\mathbf{x}$ as a special case. More generally, a graph convolutional filter

$$\mathbf{F}_{\mathcal{G}} = \mathbf{U}_G h(\mathbf{\Lambda}_G)\mathbf{U}_G^\intercal, \quad (8)$$

where $h(\cdot)$ is a polynomial of degree at most $N-1$, induces a GDS convolutional filter

$$\begin{aligned}\mathcal{F}_G(\mu) &= (\mathbf{F}_G)_*\mu = (\mathbf{U}_G h(\mathbf{\Lambda}_G)\mathbf{U}_G^\intercal)_*\mu \\ &= (\mathbf{U}_G)_* h(\mathbf{\Lambda}_G)_* (\mathbf{U}_G^\intercal)_*\mu,\end{aligned}$$

where the last equality follows from the associativity property in Proposition 1(iv). A GDS convolution can thus be viewed as a composition of three pushforward maps: a GDS-FT transports the input distribution μ to the spectral domain, where the filter

$h(\mathbf{\Lambda}_G)$ reshapes the distribution of frequency components, and finally an inverse GDS-FT transports the filtered distribution back to the vertex domain.

Example 2. *Suppose μ is a multivariate Gaussian distribution with mean $\boldsymbol{m}$ and covariance matrix $\mathbf{\Sigma}$. Applying the GDS convolution induced by the linear map $\mathbf{F}_G$, we obtain that $\mathcal{F}_G(\mu)$ is also Gaussian, with mean $\mathbf{F}_G\boldsymbol{m}$ and covariance $\mathbf{F}_G\mathbf{\Sigma}\mathbf{F}_G^\intercal$ due to the property of jointly Gaussian distributions. Hence, $\mathcal{F}_G$ modifies not only the central tendency of the signal, represented by its mean, but also its variability and dependencies, as captured by the covariance.*

Proposition 2 (Lipschitz continuity)**.** *Any graph convolutional filter $\mathbf{F}_G$ is Lipschitz continuous with respect to the Wasserstein distance, i.e.,*

$$W_p\left((\mathbf{F}_G)_*\mu, (\mathbf{F}_G)_*\nu\right) \leq \|\mathbf{F}_G\|_{\mathrm{op}} W_p(\mu,\nu) \tag{9}$$

for all $\mu, \nu \in \mathcal{P}_p(\mathbb{R}^N)$.

Proposition 2 follows immediately from (6). From (8), $\|\mathbf{F}_G\|_{\mathrm{op}} = \max_i |h(\lambda_i)|$, so the Lipschitz constant is determined by the maximum magnitude of the graph filter frequency response. Proposition 2 guarantees that the GDS convolutional filter is Lipschitz continuous with respect to the Wasserstein distance. This property is particularly relevant in practice, where the true signal distribution μ is rarely known exactly and must be approximated, e.g., by empirical distributions from finite samples or parametric fits such as Gaussian or Gaussian mixture models. This ensures that distributional approximations at the input lead to reliable approximations at the output.

C. Example Application: Graph Filter Learning

We present an illustrative graph filter learning example [3], [7] to demonstrate the GDS processing framework. Let $\mu_{\boldsymbol{\theta}} \in \mathcal{P}_p(\mathbb{R}^N)$ denote the joint distribution over all graph nodes, parameterized by a weight vector $\boldsymbol{\theta}$. In the GDS framework, filtering is formulated as the pushforward of this distribution through a graph filter $\mathbf{F}_G : \mathbb{R}^N \to \mathbb{R}^N$, yielding $\mu'_{\boldsymbol{\theta}} := (\mathbf{F}_G)_*\mu_{\boldsymbol{\theta}}$. Our objective is to identify $\mathbf{F}_G$ such that the filtered distribution $\mu'_{\boldsymbol{\theta}}$ matches a target distribution $\mu^\star$ in Wasserstein space:

$$\min_{\mathbf{F}_G} W_2((\mathbf{F}_G)_*\mu_{\boldsymbol{\theta}}, \mu^\star). \tag{10}$$

This problem formulates a graph filter learning for GDSs, where the learned filter transports the input distribution $\mu_{\boldsymbol{\theta}}$ to align with the target distribution $\mu^\star$. In this sense, $\mathbf{F}_G$ is learned at the distribution level, enabling the filter to capture graph-dependent transformations of uncertainty and correlations across nodes, rather than only manipulating individual signal realizations.

To make the optimization problem in (10) tractable, we introduce explicit parametric forms for the joint distributions $\mu_{\boldsymbol{\theta}}$ and $\mu^\star$. Specifically, we consider two representative schemes: (1) copula-based GDS filter learning (Section III-C1), in which the joint distribution is constructed by coupling prescribed marginal distributions through a copula, thereby modeling inter-node dependence separately from the marginals; and (2) GMM-based GDS filter learning (Section III-C2), in which the joint distribution is represented as a mixture of Gaussian components to provide high expressive flexibility.

1) Copula-based GDS filter learning: Assume that each node $v_i \in V$, $i = 1, \ldots, N$, is associated with a marginal distribution $\mu_i(\cdot;\boldsymbol{\theta}_i) \in \mathcal{P}_p(\mathbb{R})$, parameterized by $\boldsymbol{\theta}_i$ and estimated from local observations. Because synchronous measurements across all nodes may be unavailable, direct estimation of the joint distribution is generally infeasible. We therefore construct a joint distribution $\mu_{\boldsymbol{\theta},\kappa} \in \mathcal{P}_p(\mathbb{R}^N)$ by combining the marginals with a copula density c_κ, which captures inter-node dependence:

$$\mu_{\boldsymbol{\theta},\kappa}(x) = c_\kappa\left(F_1(x_1;\boldsymbol{\theta}_1), \ldots, F_N(x_N;\boldsymbol{\theta}_N)\right) \prod_{i=1}^N \mu_i(x_i;\boldsymbol{\theta}_i)$$

where $F_i(\cdot;\boldsymbol{\theta}_i)$ denotes the cumulative distribution function (cdf) of $\mu_i(\cdot;\boldsymbol{\theta}_i)$, $\boldsymbol{\theta} = (\boldsymbol{\theta}_i)_{i=1}^N$, and κ parametrizes the copula. By Sklar's theorem [30], [31], the marginals of $\mu_{\boldsymbol{\theta},\kappa}$ are exactly $\mu_i(\cdot;\boldsymbol{\theta}_i)$ for $i = 1, \ldots, N$.

In our GDS framework, the filtered GDS is defined as $\mu'_{\boldsymbol{\theta},\kappa} := (\mathbf{F}_G)_*\mu_{\boldsymbol{\theta},\kappa}$. We then reformulate the objective to jointly estimate the graph filter $\mathbf{F}_G$ and the copula density c_κ such that the filtered GDS $\mu'_{\boldsymbol{\theta},\kappa}$ matches a target distribution $\mu^\star$:

$$\begin{aligned} &\min_{\mathbf{F}_G,\kappa}\ W_2((\mathbf{F}_G)_*\mu_{\boldsymbol{\theta},\kappa}, \mu^\star) \\ &\text{s.t.}\ \ (\pi_i)_*\mu_{\boldsymbol{\theta},\kappa} = \mu_i, \quad i = 1, \ldots, N, \end{aligned} \tag{11}$$

where π_i denotes the projection onto the i-th coordinate. This formulation characterizes graph filter learning in which the marginals encode local uncertainty, the copula captures inter-node dependencies, and the learned filter aligns the resulting GDS with the target distribution.

To obtain an explicit form of (11), we adopt a Gaussian parameterization. Each node v_i is associated with a marginal distribution $\mu_i = \mathcal{N}(m_i, \sigma_i^2)$, where $\boldsymbol{\theta}_i = (m_i, \sigma_i^2)$ are estimated from local observations at node v_i. Inter-node dependence is modeled by a Gaussian copula with correlation matrix $\boldsymbol{R}$, which induces the joint distribution $\mu = \mathcal{N}(\boldsymbol{m}, \mathbf{\Sigma})$, where $\boldsymbol{\theta} = (\boldsymbol{m}, \mathbf{\Sigma})$, $\boldsymbol{m} = (m_1, \ldots, m_N)^\intercal$ and $\mathbf{\Sigma} = \boldsymbol{DRD}$ with $\boldsymbol{D} = \mathrm{diag}(\sigma_1, \ldots, \sigma_N)$. Applying the graph filter $\mathbf{F}_G$ to μ produces another Gaussian distribution:

$$(\mathbf{F}_G)_*\mu = \mathcal{N}(\mathbf{F}_G\boldsymbol{m}, \mathbf{F}_G\mathbf{\Sigma}\mathbf{F}_G^\intercal).$$

When the target distribution is also modeled as Gaussian, i.e., $\mu^\star = \mathcal{N}(\boldsymbol{m}^\star, \mathbf{\Sigma}^\star)$, the squared Wasserstein distance admits a closed-form expression (see Example 1). Consequently, (11) reduces to:

$$\begin{aligned} \min_{\mathbf{F}_G,\boldsymbol{R}}\ &\|\mathbf{F}_G\boldsymbol{m} - \boldsymbol{m}^\star\|_2^2 + \mathrm{Tr}\Big\{\mathbf{F}_G\mathbf{\Sigma}\mathbf{F}_G^\intercal + \mathbf{\Sigma}^\star \\ &\qquad - 2\big((\mathbf{\Sigma}^\star)^{1/2}\mathbf{F}_G\mathbf{\Sigma}\mathbf{F}_G^\intercal(\mathbf{\Sigma}^\star)^{1/2}\big)^{1/2}\Big\} \\ \text{s.t.}\ \ &\boldsymbol{R} = \boldsymbol{R}^\intercal, \quad \boldsymbol{R} \succeq \mathbf{0}, \quad \mathrm{diag}(\boldsymbol{R}) = \mathbf{1}. \end{aligned} \tag{12}$$

We solve this optimization problem using alternating minimization over $\mathbf{F}_G$ and $\boldsymbol{R}$, with each subproblem updated via gradient descent [32]. For a graph convolutional filter $\mathbf{F}_G$ of the form specified in (8), the optimization is performed over the coefficients of the polynomial $h(\cdot)$. The complete procedure is summarized in Algorithm 1.

Algorithm 1 Copula-based GDS graph filter learning algorithm

Input: Target mean $\boldsymbol{m}^\star$ and covariance $\boldsymbol{\Sigma}^\star$, marginal means $\boldsymbol{m}$, variances $\boldsymbol{D} = \mathrm{diag}(\sigma_1, \ldots, \sigma_N)$, learning rates η_1 and η_2, convergence tolerance ϵ, positive threshold δ. $\mathcal{L}$ is the objective function in (12).
Output: Optimized $\widetilde{\mathbf{F}}_G$
Initialize $\mathbf{F}_G^{(0)}$, $\boldsymbol{R}^{(0)}$, $u = 0$
repeat
  $\boldsymbol{\Sigma}^{(u)} \leftarrow \boldsymbol{D}\boldsymbol{R}^{(u)}\boldsymbol{D}$
  $\mathcal{L}^{(u)} \leftarrow$ (12)
  $\mathbf{F}_G^{(u+1)} \leftarrow \mathbf{F}_G^{(u)} - \eta_1 \nabla_{\mathbf{F}_G} \mathcal{L}^{(u)}$
  $\boldsymbol{R}^{(u+1)} \leftarrow \boldsymbol{R}^{(u)} - \eta_2 \nabla_{\boldsymbol{R}} \mathcal{L}^{(u)}$
  Project $\boldsymbol{R}^{(u+1)}$ to a valid correlation matrix:
  $\boldsymbol{R}^{(u+1)} \leftarrow \frac{1}{2}\left(\boldsymbol{R}^{(u+1)} + \boldsymbol{R}^{(u+1)\intercal}\right)$ ▷ Symmetrize
  $\boldsymbol{R}^{(u+1)} \leftarrow \boldsymbol{V}\,\mathrm{diag}(\max(\boldsymbol{\lambda}, \delta))\boldsymbol{V}^\intercal$ ▷ PSD projection
  $\boldsymbol{S} \leftarrow \mathrm{diag}\left(\sqrt{\mathrm{diag}(\boldsymbol{R}^{(u+1)})}\right)$
  $\boldsymbol{R}^{(u+1)} \leftarrow \boldsymbol{S}^{-1}\boldsymbol{R}^{(u+1)}\boldsymbol{S}^{-1}$ ▷ Normalize
  $\mathrm{diag}(\boldsymbol{R}^{(u+1)}) \leftarrow \mathbf{1}$ ▷ Set diagonal
  $u \leftarrow u + 1$
until $\|\mathcal{L}^{(u)} - \mathcal{L}^{(u-1)}\| \le \epsilon$

2) GMM-based GDS filter learning: To balance expressive power and analytical tractability, we propose to model the joint distribution across all graph nodes using a GMM. Specifically, we assume

$$\mu_{\boldsymbol{\theta}} = \sum_{k=1}^{K} a_k \xi_k \in \mathrm{GMM}_K(\mathbb{R}^N), \tag{13}$$

where each component ξ_k is a multivariate Gaussian $\xi_k = \mathcal{N}(\boldsymbol{m}_k, \boldsymbol{\Sigma}_k)$, and the mixture weights satisfy $a_k \ge 0$ and $\sum_{i=1}^K a_k = 1$.

With this model, the marginal distribution of the i-th node $\mu_i := (\pi_i)_* \mu_{\boldsymbol{\theta}}$ is a univariate GMM with the same mixture weights, i.e.,

$$\mu_i = \sum_{k=1}^{K} a_k \mathcal{N}(m_{ik}, \sigma_{ik}^2), \quad i = 1, \ldots, N, \tag{14}$$

where m_{ik} and σ_{ik}^2 denote the mean and variance of the i-th coordinate under the k-th Gaussian component ξ_k. Moreover, within each component k, the dependence structure is characterized by a Gaussian copula with correlation matrix $\mathbf{R}_k$. Equivalently, the covariance can be decomposed as $\boldsymbol{\Sigma}_k = \mathbf{D}_k \mathbf{R}_k \mathbf{D}_k$ with $\mathbf{D}_k := \mathrm{diag}(\sigma_{1k}, \cdots, \sigma_{nk})$, and the component mean vector is $\boldsymbol{m}_k = (m_{1k}, \cdots, m_{Nk})^\intercal$.

Similarly, the target distribution is modeled as $\mu^\star = \sum_{l=1}^{L} b_l \xi_l^\star \in \mathrm{GMM}_L(\mathbb{R}^N)$ with at most L Gaussian components, where each component is given by $\xi_l^\star = \mathcal{N}(\boldsymbol{m}_l^\star, \boldsymbol{\Sigma}_l^\star)$. Under these assumptions, the filter learning problem (10) is

$$\begin{aligned} &\min_{\mathbf{F}_G} \; W_2((\mathbf{F}_G)_* \mu_{\boldsymbol{\theta}}, \mu^\star) \\ &\text{s.t. } \; \mu_{\boldsymbol{\theta}} \in \mathrm{GMM}_K(\mathbb{R}^N) \text{ with } (\pi_i)_* \mu_{\boldsymbol{\theta}} = \mu^{(i)} \\ &\qquad \text{and } \mu^\star \in \mathrm{GMM}_L(\mathbb{R}^N), \end{aligned} \tag{15}$$

where $(\mathbf{F}_G)_* \mu_{\boldsymbol{\theta}} = \sum_{k=1}^K a_k (\mathbf{F}_G)_* \xi_k$.

For tractability, we approximate the Wasserstein distance W_2 by the Mixture-Wasserstein distance MW_2 defined in (4). It admits efficient computation via component-wise optimal transport and provides a practical surrogate for W_2 [20], [29], [33]. This leads to the following relaxed formulation:

$$\begin{aligned} &\min_{\mathbf{F}_G, \{\mathbf{R}_k\}_{k=1}^K, \boldsymbol{\omega} \in \Pi(\mathbf{a}, \mathbf{b})} \; \sum_{k,l} \boldsymbol{\omega}_{kl} W_2^2((\mathbf{F}_G)_* \xi_k, \xi_l^\star) \\ &\text{s.t. } \; \mathbf{a} = (a_1, \ldots, a_K)^\intercal, \mathbf{b} = (b_1, \ldots, b_L)^\intercal \\ &\quad \Pi(\mathbf{a}, \mathbf{b}) = \{\boldsymbol{\omega} \in \mathbb{R}_+^{K \times L} : \boldsymbol{\omega}\mathbf{1} = \mathbf{a} \text{ and } \boldsymbol{\omega}^\intercal \mathbf{1} = \mathbf{b}\} \\ &\quad \mathbf{R}_k = \mathbf{R}_k^\intercal, \quad \mathbf{R}_k \succeq \mathbf{0}, \quad \mathrm{diag}(\mathbf{R}_k) = \mathbf{1}, \forall\, k. \end{aligned} \tag{16}$$

Here, $W_2((\mathbf{F}_G)_* \xi_k, \xi_l^\star)^2$ admits the close-form expression:

$$\begin{aligned} &W_2^2((\mathbf{F}_G)_* \xi_k, \xi_l^\star) = \|\mathbf{F}_G \boldsymbol{m}_k - \boldsymbol{m}_l^\star\|_2^2 \\ &+ \mathrm{Tr}\Big\{\mathbf{F}_G \boldsymbol{\Sigma}_k \mathbf{F}_G^\intercal + \boldsymbol{\Sigma}_l^\star - 2\big((\boldsymbol{\Sigma}_l^\star)^{1/2} \mathbf{F}_G \boldsymbol{\Sigma}_k \mathbf{F}_G^\intercal (\boldsymbol{\Sigma}_l^\star)^{1/2}\big)^{1/2}\Big\}. \end{aligned} \tag{17}$$

We solve this problem via alternating minimization. Specifically, we update the graph filter $\mathbf{F}_G$ and the correlation matrices $\{\mathbf{R}_k\}_{k=1}^K$ using gradient descent, while recomputing the transport plan $\boldsymbol{\omega}$ at each iteration by solving the entropically regularized optimal transport problem [20], [33], i.e.,

$$\boldsymbol{\omega}^\star \in \underset{\boldsymbol{\omega} \in \Pi(\mathbf{a}, \boldsymbol{b})}{\arg\min} \; \langle \boldsymbol{\omega}, \mathbf{C} \rangle + \varepsilon \sum_{k,l} \boldsymbol{\omega}_{kl}(\log \boldsymbol{\omega}_{kl} - 1), \tag{18}$$

where $\mathbf{C}$ is the cost matrix (i.e., $\mathbf{C}_{kl} = W_2^2((\mathbf{F}_G)_* \xi_k, \xi_l^\star)$) defined in (17), $\varepsilon > 0$ is the entropic regularization parameter, $\Pi(\mathbf{a}, \boldsymbol{b})$ denotes the set of couplings with prescribed marginals $\mathbf{a}$ and $\boldsymbol{b}$, and $\langle \cdot, \cdot \rangle$ denotes the Frobenius inner product. We compute $\boldsymbol{\omega}^\star$ efficiently using the Sinkhorn algorithm [34], [35]. The overall procedure is summarized in Algorithm 2.

IV. The Generalized GDS Framework

We next generalize the GDS processing framework introduced in Section III by allowing the graph topology to follow a signal-dependent distribution [18].

A. Signal Adaptive Graph Structures

We propose to treat the graph as a data-dependent representation whose connectivity varies with the observed signal (see Fig. 2). In practice, statistical dependencies among nodes are often induced by latent physical or functional mechanisms that manifest in the measurements themselves. Consequently, a graph constructed from the data—e.g., by linking nodes with strong correlation or coherence—may vary across signal realizations, even when the vertex set and sensing locations remain fixed. This motivates modeling the graph as a *signal-adaptive* (and potentially random) object: given a graph signal $\mathbf{x} \in \mathbb{R}^N$, we associate with it a conditional distribution $\nu_{\mathbf{x}}$ over graphs that captures the plausible connectivity patterns consistent with $\mathbf{x}$. We formalize this notion via *SAGSs*. Throughout this paper, we view $\mathcal{G}_N$ as parametrized by adjacency matrices, and identified with a Euclidean space.

Definition 5 (Signal adaptive graph structure (SAGS))**.** *Let $V = \{v_1, \ldots, v_N\}$ be an ordered set of N vertices, and let $\mathcal{G}_N$*

Algorithm 2 GMMs-based GDS graph filter learning algorithm

Input: Source GMM $\{(\boldsymbol{m}_k, \boldsymbol{\Sigma}_k, a_k)\}_{k=1}^K$, target GMM $\{(\boldsymbol{m}_l^\star, \boldsymbol{\Sigma}_l^\star, b_l)\}_{l=1}^L$, learning rate η_1 and η_2, convergence tolerance ϵ, regularization coefficient ε, positive threshold δ. $\mathcal{L}$ is the objective function in (16).
Output: Optimized $\widetilde{\mathbf{F}}_G$
Initialize $\mathbf{F}_G^{(0)}$, $(\boldsymbol{R}_k^{(0)})_{k=1}^K$ and $u = 0$
repeat
  $W_2^2((\mathbf{F}_G^{(u)})_*\xi_k, \xi_l^\star)^2 \leftarrow$ (17) ▷ Compute cost matrix
  $\boldsymbol{\omega}^{(u)} \leftarrow$ (18) ▷ Update transport plan
  $\mathcal{L}^{(u)} \leftarrow$ compute (16) with $\boldsymbol{\omega}^{(u)}$ ▷ Update loss
  $\mathbf{F}_G^{(u+1)} \leftarrow \mathbf{F}_G^{(u)} - \eta_1 \nabla_{\mathbf{F}_G} \mathcal{L}^{(u)}$
  for $k = 1, \ldots, K$ **do**
    $\boldsymbol{R}_k^{(u+1)} \leftarrow \boldsymbol{R}_k^{(u)} - \eta_2 \nabla_{\boldsymbol{R}_k} \mathcal{L}^{(u)}$
    Project $\boldsymbol{R}_k^{(u+1)}$ to a valid correlation matrix:
    $\boldsymbol{R}_k^{(u+1)} \leftarrow \frac{1}{2}\left(\boldsymbol{R}_k^{(u+1)} + \boldsymbol{R}_k^{(u+1)^\intercal}\right)$ ▷ Symmetrize
    $\boldsymbol{R}_k^{(u+1)} \leftarrow \boldsymbol{V}_k \operatorname{diag}(\max(\boldsymbol{\lambda}_k, \delta))\boldsymbol{V}_k^\intercal$ ▷ PSD
    $\boldsymbol{S}_k \leftarrow \operatorname{diag}\left(\sqrt{\operatorname{diag}(\boldsymbol{R}_k^{(u+1)})}\right)$
    $\boldsymbol{R}_k^{(u+1)} \leftarrow \boldsymbol{S}_k^{-1}\boldsymbol{R}_k^{(u+1)}\boldsymbol{S}_k^{-1}$ ▷ Normalize
    $\operatorname{diag}(\boldsymbol{R}_k^{(u+1)}) \leftarrow \mathbf{1}$ ▷ Set diagonal
  end for
  $u \leftarrow u + 1$
until $\|\mathcal{L}^{(u)} - \mathcal{L}^{(u-1)}\| \le \epsilon$

denote the space of all weighted graphs on the fixed vertex set V. A SAGS $\mathcal{A}$ is, for each $\mathbf{x} \in \mathbb{R}^N$, a conditional probability distribution $\nu_{\mathbf{x}}(\cdot) = \mathcal{A}(\mathbf{x}, \cdot) \in \mathcal{P}_p(\mathcal{G}_N)$. ▷ $G \mid \mathbf{x} \sim \nu_{\mathbf{x}}$

More precisely, adopting probability-theoretic notations [22, Section 4.1.3], for any Borel set $B \subseteq \mathcal{G}_N$, $\mathcal{A}(\mathbf{x}, B)$ is a version of $\mathbb{P}(G \in B \mid \sigma(\mathbf{x}))$, where $\sigma(\mathbf{x})$ denotes the σ-algebra generated by the random element $\mathbf{x}$. Moreover, for *each* $\mathbf{x}$, $\nu_{\mathbf{x}}(\cdot) := \mathcal{A}(\mathbf{x}, \cdot)$ defines a probability measure on $\mathcal{G}_N$. Note that in this work, for simplicity, we assume that $\nu_{\mathbf{x}}$ is well-defined for every $\mathbf{x} \in \mathbb{R}^N$, instead of only for μ-a.e. $\mathbf{x}$. This simplification avoids dependency of $\mathcal{A}$ on μ, and measure-theoretic difficulties, which require additional technical assumptions to resolve. In the sequel, we adopt the simplified notation introduced in Definition 5.

If $\nu_{\mathbf{x}} = \nu$ for all $\mathbf{x}$ (i.e., it is independent of $\mathbf{x}$), we call it a constant SAGS [18]. Moreover, if $\nu_{\mathbf{x}} = \delta_G$ for a fixed graph $G \in \mathcal{G}_N$, then the SAGS framework reduces to the classical GSP setting with a single deterministic underlying graph.

For any $\mu \in \mathcal{P}_p(\mathbb{R}^N)$, we have an associated joint distribution $\mathcal{A}^*\mu$ on $\mathbb{R}^N \times \mathcal{G}_N$, given by

$$(\mathcal{A}^*\mu)(B) = \int_B \mathrm{d}\nu_{\mathbf{x}}(G)\,\mathrm{d}\mu(\mathbf{x}) \tag{19}$$

for any Borel set $B \subseteq \mathbb{R}^N \times \mathcal{G}_N$. This is the pullback map of distributions $\mathcal{P}_p(\mathbb{R}^N) \to \mathcal{P}_p(\mathbb{R}^N \times \mathcal{G}_N)$ (i.e., the joint distribution of $(\mathbf{x}, G)$ in the p-th order Wasserstein space), as confirmed by the following result.

Lemma 1. *For any GDS $\mu \in \mathcal{P}_p(\mathbb{R}^N)$ and SAGS $\mathcal{A}$ such that*

$$\int_{\mathbb{R}^N} W_p^p(\nu_{\mathbf{x}}, \delta_{G_0})\,\mathrm{d}\mu(\mathbf{x}) < \infty \tag{20}$$

for some fixed $G_0 \in \mathcal{G}_N$, the distribution $\mathcal{A}^*\mu$ defined in (19) *belongs to $\mathcal{P}_p(\mathbb{R}^N \times \mathcal{G}_N)$.* ▷ $(\mathbf{x}, G) \sim \mathcal{A}^*\mu$

Proof: See Section B in the Appendix. ■

An SAGS $\mathcal{A}$ encodes the structural information of the underlying graph in a signal-dependent manner. For a given signal $\mathbf{x}$, it determines the plausible graph structures on V through the measure $\nu_{\mathbf{x}}$. This concept is illustrated in Fig. 2. The next subsection describes how GDS transformations are performed under this signal-adaptive graph structure, extending the framework of Section III.

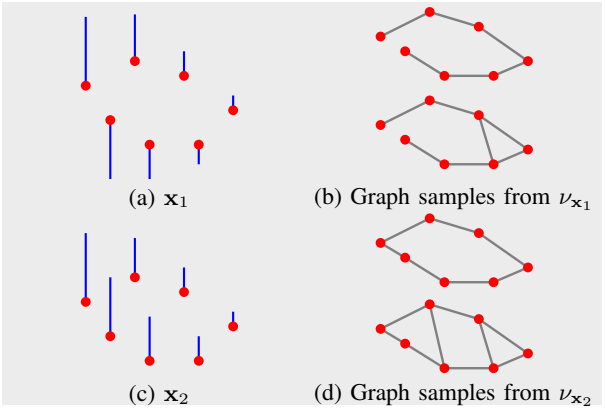

Fig. 2. An illustration of SAGS. For two distinct signals $\mathbf{x}_1, \mathbf{x}_2$, the likelihood of a graph structure is determined by the smoothness of the signal on that structure, resulting in distinct distributions $\nu_{\mathbf{x}_1}, \nu_{\mathbf{x}_2}$. (a)(c) Two distinct signals. (b)(d) Representative graph structures sampled from $\nu_{\mathbf{x}_1}$ and $\nu_{\mathbf{x}_2}$, respectively.

B. Generalized GDS Processing Framework

1) Generalized GDS transforms: We extend the GDS Fourier transform and GDS convolutional filtering to the SAGS setting. These operations, referred to as the generalized GDS Fourier transform and generalized GDS convolutional filtering, are defined below.

Definition 6 (Generalized GDS Fourier transform)**.** *For a given graph signal $\mathbf{x} \in \mathbb{R}^N$ and graph $G \in \mathcal{G}_N$, let $\Phi(\mathbf{x}, G) := \mathbf{U}_G^\intercal \mathbf{x}$ denote the GFT of $\mathbf{x}$ with respect to G. For a GDS $\mu \in \mathcal{P}_p(\mathbb{R}^N)$ and a SAGS $\mathcal{A}$, the generalized* GDS-FT *is the pushforward measure*

$$\hat{\mu} := (\Phi_* \circ \mathcal{A}^*)\mu, \tag{21}$$

i.e., for any Borel set $B \in \mathcal{B}(\mathbb{R}^N)$,

$$\begin{aligned}\widehat{\mu}(B) &= (\mathcal{A}^*\mu)\left(\Phi^{-1}(B)\right) \\ &= (\mathcal{A}^*\mu)(\{(\mathbf{x}, G) \,:\, \mathbf{U}_G^\intercal \mathbf{x} \in B\}).\end{aligned} \tag{22}$$

▷ $\mathbf{x} \sim \mu,\ G \mid \mathbf{x} \sim \nu_{\mathbf{x}},\ \mathbf{U}_G^\intercal \mathbf{x} \sim \hat{\mu}$

Intuitively, the generalized GDS-FT transforms a distribution from the vertex domain to the frequency domain by jointly accounting for both the signal and the underlying graph structure through the joint distribution $\mathcal{A}^*\mu$. For each pair

$(\mathbf{x}, G)$ drawn from the distribution $\mathcal{A}^*\mu$, the signal $\mathbf{x}$ is projected onto the eigenbasis $\mathbf{U}_G$ of the corresponding graph, and the resulting distribution of these projections defines $\widehat{\mu}$.

Definition 7 (Generalized GDS convolutional filter)**.** *Let $\mathbf{F}_G$ be a graph convolutional filter (i.e., a polynomial of $\mathbf{S}_G$) for each graph $G \in \mathcal{G}_N$ and let*

$$\mathcal{J} : \mathbb{R}^N \times \mathcal{G}_N \to \mathbb{R}^N, \quad (\mathbf{x}, G) \mapsto \mathbf{F}_G\mathbf{x}. \tag{23}$$

For a SAGS $\mathcal{A}$, a generalized GDS convolutional filter *is a mapping $\mathcal{T} := \mathcal{T}_{\mathcal{J},\mathcal{A}}$ defined by*

$$\mathcal{T} : \mathcal{P}_p(\mathbb{R}^N) \to \mathcal{P}_p(\mathbb{R}^N), \quad \mu \mapsto (\mathcal{J}_* \circ \mathcal{A}^*)\mu. \tag{24}$$

I.e., for any Borel set $B \in \mathcal{B}(\mathbb{R}^N)$, the filter output yields

$$\begin{aligned}\mathcal{T}(\mu)(B) &= (\mathcal{A}^*\mu)\left(\mathcal{J}^{-1}(B)\right) \\ &= (\mathcal{A}^*\mu)(\{(\mathbf{x}, G) \,:\, \mathbf{F}_G\mathbf{x} \in B\}).\end{aligned}$$

$\triangleright\ \mathbf{x} \sim \mu,\ G \mid \mathbf{x} \sim \nu_{\mathbf{x}},\ \mathcal{J}(\mathbf{x}, G) = \mathbf{F}_G\mathbf{x} \sim \mathcal{T}(\mu)$

Analogously to the Fourier transform, a generalized GDS convolutional filter maps an input GDS μ to the filtered GDS defined as the distribution of $\mathbf{Y} = \mathbf{F}\mathbf{x}$, where $(\mathbf{x}, G)$ is drawn from the joint distribution $\mathcal{A}^*\mu$. The filter thus propagates uncertainty in both the signal and the graph topology through the same local aggregation mechanism as classical graph filtering, applied pointwise to each realization of $(\mathbf{x}, G)$. In particular, when the graph is deterministic, i.e., $\nu_{\mathbf{x}} = \delta_G$, both Definitions 3 and 4 are recovered as special cases.

Table I presents a dictionary that maps core concepts of traditional GSP to their counterparts in the proposed generalized GDS framework. Using this dictionary, existing GSP models and formulations can be systematically translated into the generalized GDS setting.

TABLE I
MAPPING BETWEEN GSP AND GDS

Traditional GSP	GDS framework
Signal	GDS (Definition 2): μ
Graph	SAGS (Definition 5): $\mathcal{A}$
GFT	Generalized GDS-FT (Definition 6)
Filter	Generalized GDS filter (Definition 7)

C. Analytic Properties Of Generalized GDS Transforms

In this subsection, we study the analytic properties of generalized GDS transforms, which provide the theoretical foundation for modeling GDSs with empirical or mixed Gaussian distributions. To establish the main results in a unified framework, we first introduce a general notion of GDS transformation under which both the generalized GDS Fourier transform and convolutional filters arise as special cases. Recall that $M_N(\mathbb{R})$ denotes the normed space of $N \times N$ real matrices with the operator norm.

Definition 8. *Given a SAGS $\mathcal{A}$ and a matrix-valued function $\mathbf{M}_{(\cdot)} : G \in \mathcal{G}_N \mapsto \mathbf{M}_G \in M_N(\mathbb{R})$, the generalized GDS transformation $\mathcal{T}$ associated with $(\mathcal{A}, \mathbf{M}_{(\cdot)})$ is as defined in Definition 7 with $\mathbf{F}_G$ replaced by $\mathbf{M}_G$, i.e.,*

$$\mathcal{J} : \mathbb{R}^N \times \mathcal{G}_N \to \mathbb{R}^N, \quad (\mathbf{x}, G) \mapsto \mathbf{M}_G\mathbf{x}. \tag{25}$$

$\triangleright\ \mathbf{x} \sim \mu,\ G \mid \mathbf{x} \sim \nu_{\mathbf{x}},\ \mathcal{J}(\mathbf{x}, G) = \mathbf{M}_G\mathbf{x} \sim \mathcal{T}(\mu)$

For example, the GDS-FT is associated with $\mathbf{M}_G = \mathbf{U}_G^{\mathsf{T}}$, while a generalized GDS convolutional filter corresponds to $\mathbf{M}_G = \mathbf{F}_G$. In both cases, the GDS transformation is defined by the pushforward of the joint distribution $\mathcal{A}^*\mu$ through the map $\mathcal{J} : \mathbb{R}^N \times \mathcal{G}_N \to \mathbb{R}^N$, which maps each graph G to its associated matrix $\mathbf{M}_G$ and then applies $\mathbf{M}_G$ to $\mathbf{x}$.

TABLE II
A SUMMARY OF THE MAIN MAPS. IN THE LAST COLUMN, $\mathfrak{L}(\cdot)$ IS THE PROBABILITY DISTRIBUTION OF ITS ARGUMENT.

Operator	Mapping	Eqn.	R.v.
$\mathcal{A}^*$	$\mathcal{P}_p(\mathbb{R}^N) \to \mathcal{P}_p(\mathbb{R}^N \times \mathcal{G}_N)$	(19)	$\mathfrak{L}(\mathbf{x}) \mapsto \mathfrak{L}(\mathbf{x}, G)$
$\mathcal{J}$	$\mathbb{R}^N \times \mathcal{G}_N \to \mathbb{R}^N$	(25)	$(\mathbf{x}, G) \mapsto \mathbf{M}_G\mathbf{x}$
$\mathcal{T} = \mathcal{J}_* \circ \mathcal{A}^*$	$\mathcal{P}_p(\mathbb{R}^N) \to \mathcal{P}_p(\mathbb{R}^N)$	(24)	$\mathfrak{L}(\mathbf{x}) \mapsto \mathfrak{L}(\mathbf{M}_G\mathbf{x})$
$\mathcal{M}$	$\mathbb{R}^N \to \mathcal{P}_p(M_N(\mathbb{R}))$	(26)	$\mathbf{x} \mapsto \mathfrak{L}(\mathbf{M}_G)$

Definition 9 (Induced transform distribution)**.** *Consider a generalized GDS transformation $\mathcal{T}$ associated with $(\mathcal{A}, \mathbf{M}_{(\cdot)})$. Let*

$$\mathcal{M} : \mathbb{R}^N \to \mathcal{P}_p(M_N(\mathbb{R})) \tag{26}$$

be the map that assigns to each $\mathbf{x} \in \mathbb{R}^N$ the distribution of the matrix $\mathbf{M}_G$, where G is drawn from the SAGS $\nu_{\mathbf{x}}(\cdot) = \mathcal{A}(\mathbf{x}, \cdot)$. Formally, $\mathcal{M}(\mathbf{x})$ is the pushforward of $\nu_{\mathbf{x}} \in \mathcal{P}_p(\mathcal{G}_N)$ through $G \mapsto \mathbf{M}_G$. We call $\mathcal{M}(\mathbf{x})$ the induced transform distribution *of $\mathbf{x}$ under the generalized GDS transformation $\mathcal{T}$.*
$\triangleright\ \mathbf{x} \sim \mu,\ G \mid \mathbf{x} \sim \nu_{\mathbf{x}},\ \mathbf{M}_G \sim \mathcal{M}(\mathbf{x})$

We can now state the key continuity properties of the generalized GDS transforms $\mathcal{T}$ given appropriate conditions in $\mathcal{M}$. For easy reference, the maps introduced in this section are summarized in Table II.

Theorem 1 (Uniform continuity on compact sets)**.** *Let $M_N(\mathbb{R})$ be endowed with the operator norm. Suppose $C \subset \mathbb{R}^N$ is compact, and the map $\mathcal{M} : \mathbb{R}^N \to \mathcal{P}_p(M_N(\mathbb{R}))$ in Definition 9 is continuous on C. Then the generalized GDS transform $\mathcal{T} : \mathcal{P}_p(C) \to \mathcal{P}_p(\mathbb{R}^N)$ in Definition 8 is uniformly continuous.*

Proof: See Section C in the Appendix. ∎

In many practical settings, it is natural to assume that signals lie in a compact subset of $\mathbb{R}^N$. Under this assumption, continuity of $\mathcal{M}$ is a mild requirement. Specifically, the domain of $\mathcal{M}$ is C, whereas the domain of $\mathcal{T}$ is $\mathcal{P}_2(C)$. Since $\mathcal{M}$ is an intermediate object in the construction of $\mathcal{T}$, establishing its continuity is generally easier. A representative example is the constant SAGS case [18], where $\nu_{\mathbf{x}} = \nu$ is independent of $\mathbf{x}$; consequently, $\mathcal{M}(\mathbf{x}) = (\mathbf{M}_{(\cdot)})_*\nu$ is constant in $\mathbf{x}$ and therefore trivially continuous.

Theorem 2 (Pointwise continuity under Lipschitz condition)**.** *Suppose the map $\mathcal{M} : \mathbb{R}^N \to \mathcal{P}_p(M_N(\mathbb{R}))$ in Definition 9 is Lipschitz continuous. Then, the generalized GDS transform*

$\mathcal{T} : \mathcal{P}_{2p}(\mathbb{R}^N) \to \mathcal{P}_p(\mathbb{R}^N)$ in Definition 8 is continuous at any $\mu \in \mathcal{P}_{2p}(\mathbb{R}^N)$ (from the W_{2p} topology in the domain to the W_p topology in the codomain).

Proof: See Section D in the Appendix. ∎

Both finite atomic measures [20, Theorem 6.18] and GMMs [36] are dense in $\mathcal{P}_p(\mathbb{R}^N)$ under W_p for every $1 \le p < \infty$. Therefore, continuity of $\mathcal{T}$ in Theorems 1 and 2 implies that its behavior on empirical measures (constructed from finitely many samples) or GMMs closely approximates its behavior on the true underlying distribution. Consequently, for practical applications (e.g., Section IV-D), it is sufficient to work with empirical measures or GMMs, which are tractable both conceptually and computationally.

Moreover, these continuity results provide a stability guarantee for GDS transforms: small perturbations of the input signal distribution arising from measurement noise, distribution shift, or finite-sample approximation, lead to controlled perturbations of the output. On compact signal domains, this stability holds with respect to W_p. In the noncompact case, Theorem 2 establishes continuity from W_{2p} to W_p, reflecting the need to control higher-order tails when the graph-dependent transform can grow with the signal magnitude. This condition covers important distribution classes, including compactly supported distributions and GMMs.

D. Example Application: Anomaly Detection

In classical GSP, anomaly detection applies a high-pass graph filter and flags anomalies when high-frequency GFT coefficients exceed a threshold calibrated from normal data [37]. However, this approach disregards the distributional structure of high-frequency components, rendering it sensitive to noise and susceptible to false alarms under distribution shifts. To address this limitation, we propose a generalized GDS-based formulation that characterizes the empirical distribution of high-frequency features and detects anomalies by comparing the test distribution against a reference distribution estimated from normal data.

Consider a binary anomaly detection problem with class set $\mathcal{C} = \{\text{normal}, \text{abnormal}\}$. For each class $c \in \mathcal{C}$, let $\{\mathbf{x}_m^{(c)}, G_m^{(c)}\}_{m=1}^M$ denote independent and identically distributed (i.i.d.) signal-graph observations with $\mathbf{x}_m^{(c)} \sim \mu^{(c)}$. We assume the SAGS $\mathcal{A}$ is common to both classes, so that the two classes share the same signal-to-graph mapping $\mathbf{x} \mapsto \nu_{\mathbf{x}}$. Consequently, differences between the class-conditional joint distributions $\mathcal{A}^*\mu^{(\text{normal})}$ and $\mathcal{A}^*\mu^{(\text{abnormal})}$ arise solely from $\mu^{(\text{normal})} \neq \mu^{(\text{abnormal})}$.

To extract anomaly-sensitive features, we apply the GFT to map each signal to the spectral domain. Define $\Phi : \mathbb{R}^N \times \mathcal{G}_N \to \mathbb{R}^N$ by $\Phi(\mathbf{x}, G) = \mathbf{U}_G^{\mathsf{T}}\mathbf{x}$, where $\mathbf{U}_G$ denotes the graph Fourier eigenbasis of G with respect to a GSO $\mathbf{S}_G$. Because anomalies are expected to manifest primarily in high-frequency components, let $\mathcal{I} = \{i : \lambda_1 \le i \le \lambda_2\}$ denote a selected high-frequency index set. For each $i \in \mathcal{I}$, let $\pi_i : \mathbb{R}^N \to \mathbb{R}$, $\pi_i(\mathbf{v}) = v_i$, denote the coordinate projection onto the i-th graph Fourier coefficient. For each class $c \in \mathcal{C}$, the induced high-frequency characteristic distribution is defined as

$$\mu_{\text{HF}}^{(c)} := \frac{1}{|\mathcal{I}|}\sum_{i\in\mathcal{I}}(\pi_i \circ \Phi)\mathcal{A}^*\mu^{(c)}. \tag{27}$$

In practice, $\mu_{\text{HF}}^{(c)}$ is unknown and is estimated from training data by fitting a one-dimensional GMM to the collected high-frequency coefficient samples. This distribution captures the statistical signature of high-frequency spectral components for class c. Because anomalous signals are expected to induce stronger graph-irregular variations, normal and abnormal signals may yield distinct high-frequency coefficient distributions. Consequently, $\mu_{\text{HF}}^{(c)}$ serves as a discriminative distributional feature for anomaly detection. The procedure consists of the following steps.

a) Step 1: Estimate reference distribution: Assume $\{\mathbf{x}_m^{(\text{normal})}\}_{m=1}^M$ is split into three disjoint sets: $\mathcal{D}_{\text{train}}$ for estimating the reference distribution, $\mathcal{D}_{\text{cal}}$ for threshold calibration, and $\mathcal{D}_{\text{test}}$ for evaluation. We estimate the reference distribution from $\mathcal{D}_{\text{train}}$ as a K-component GMM, i.e.,

$$\hat{\mu}_{\text{HF}}^{\text{ref}} := \sum_{k=1}^K \alpha_k \mathcal{N}\left(m_k^{(\text{ref})}, \left(\sigma_k^{(\text{ref})}\right)^2\right) \in \mathcal{P}(\mathbb{R}),$$

where α_k, $m_k^{(\text{ref})}$ and $\sigma_k^{(\text{ref})}$ are estimated from high-frequency coefficient samples $\{(\pi_i \circ \Phi)(\mathbf{x}_m, G_m) \mid \mathbf{x}_m \in \mathcal{D}_{\text{train}},\ G_m \sim \nu_{\mathbf{x}_m},\ i \in \mathcal{I}\}$.

b) Step 2: Calibrate detection threshold: Partition $\mathcal{D}_{\text{cal}}$ into N_B^{cal} batches $\{B_b^{\text{cal}}\}_{b=1}^{N_B^{\text{cal}}}$, each of size $|B_b^{\text{cal}}| = n$. For each batch, we estimate its high-frequency distribution as an L-component GMM, i.e.,

$$\hat{\mu}_{\text{HF}}^{\text{cal},b} := \sum_{\ell=1}^L \alpha'_\ell \mathcal{N}\left(m_\ell^{(b)}, \left(\sigma_\ell^{(b)}\right)^2\right) \in \mathcal{P}(\mathbb{R}),$$

where α_l, $m_\ell^{(b)}$ and $\sigma_\ell^{(b)}$ are estimated from $\{(\pi_i \circ \Phi)(\mathbf{x}_m, G_m) \mid \mathbf{x}_m \in B_b^{\text{cal}}, G_m \sim \nu_{\mathbf{x}_m},\ i \in \mathcal{I}\}$. The number of components L is chosen independently of K, as the reference and per-batch GMMs are fitted separately. The calibration score is then computed as $d_b := d(\hat{\mu}_{\text{HF}}^{\text{ref}}, \hat{\mu}_{\text{HF}}^{\text{cal},b})$, where $d(\cdot,\cdot)$ measures the discrepancy between two GMMs: either via a simple surrogate statistic based on component means, or via a more principled distributional distance (e.g., mixture Wasserstein distance). Specifically, we consider the following two choices:

- Peak location distance:

$$\begin{aligned} d(\hat{\mu}_{\text{HF}}^{\text{ref}}, \hat{\mu}_{\text{HF}}^{\text{cal},b}) = \frac{1}{2}\Big(&\frac{1}{L}\sum_{\ell=1}^L \min_k \|m_\ell^{(b)} - m_k^{(\text{ref})}\|_2 \\ &+ \frac{1}{K}\sum_{k=1}^K \min_\ell \|m_\ell^{(b)} - m_k^{(\text{ref})}\|_2\Big). \end{aligned} \tag{28}$$

- Mixture Wasserstein distance:

$$d(\hat{\mu}_{\text{HF}}^{\text{ref}}, \hat{\mu}_{\text{HF}}^{\text{cal},b}) = MW_2(\hat{\mu}_{\text{HF}}^{\text{ref}}, \hat{\mu}_{\text{HF}}^{\text{cal},b})^2. \tag{29}$$

Finally, set the detection threshold as

$$\tau = \text{Quantile}_{1-\alpha}\left(\{d_b\}_{b=1}^{N_B^{\text{cal}}}\right),$$

with significance level α.

c) Step 3: Detection rule: Given a test batch, we estimate its high-frequency distribution $\hat{\mu}_{\mathrm{HF}}^{\mathrm{test}}$ as in Step 2, and classify it by comparing its discrepancy from the reference against the calibrated threshold τ:

$$\hat{c} = \begin{cases} \text{normal}, & d(\hat{\mu}_{\mathrm{HF}}^{\mathrm{ref}}, \hat{\mu}_{\mathrm{HF}}^{\mathrm{test}}) \le \tau, \\ \text{abnormal}, & d(\hat{\mu}_{\mathrm{HF}}^{\mathrm{ref}}, \hat{\mu}_{\mathrm{HF}}^{\mathrm{test}}) > \tau. \end{cases}$$

We apply the scheme on a real dataset in Section V-B.

V. Numerical Experiments

A. Graph Filter Learning

1) Dataset and Experiment setup: We evaluate both *GDS-Cop* and *GDS-GMMs* on a COVID-19 dataset from The New York Times.[1] We use records for California's $N = 58$ counties from July 29, 2020, to August 1, 2022, splitting them into a training set $\mathcal{D}_{\mathrm{train}}$ (July 29, 2020–July 30, 2021) and a test set $\mathcal{D}_{\mathrm{test}}$ (July 31, 2021–August 1, 2022). Counties are nodes with edges defined by geographic adjacency. Both training and test sets are evenly partitioned into $\mathcal{S}$ non-overlapping time windows, i.e., $\mathcal{D}_{\mathrm{train}} = \{f_{\mathrm{train}}(V, \mathcal{T}_s)\}_{s=1}^{\mathcal{S}}$, where $f_{\mathrm{train}}(V, \mathcal{T}_s)$ denotes the number of cases reports across V during the s-th time window $\mathcal{T}_s$. Each window $\mathcal{T}_s$ consists of $\mathcal{W}$ consecutive days, so that the window size is given by $\mathcal{W} = |\mathcal{T}_s|$.

For *GDS-Cop*, during training, the target statistics, namely mean $\boldsymbol{m}^\star$ and covariance $\boldsymbol{\Sigma}^\star$, are estimated from the subsequent window $f_{\mathrm{train}}(V, \mathcal{T}_{s+1})$ following the input window $f_{\mathrm{train}}(V, \mathcal{T}_s)$. The marginal mean m_i and variance σ_i for each node v_i are computed from its local observations $f_{\mathrm{train}}(v_i, \mathcal{T}_s)$. After optimizing $\widetilde{\mathbf{F}}_G$ using (12), we evaluate it on the test set. For *GDS-GMMs*, by contrast, we directly estimate a joint Gaussian mixture model from the multivariate observations over the entire graph within each time window. Specifically, given the samples $f_{\mathrm{train}}(V, \mathcal{T}_s)$, we fit a joint GMM to obtain the mixture weights $\{a_k\}_{k=1}^K$, component means $\{\boldsymbol{m}_k\}_{k=1}^K$ and covariances $\{\boldsymbol{\Sigma}_k\}_{k=1}^K$, where K is a hyperparameter controlling the number of Gaussian components. The target distribution is estimated analogously from the subsequent window $f_{\mathrm{train}}(V, \mathcal{T}_{s+1})$, yielding the parameters $\{\boldsymbol{m}_l^\star, \boldsymbol{\Sigma}_l^\star, b_l\}_{l=1}^L$, where L is a hyperparameter controlling the number of Gaussian components. These joint GMM parameters (i.e., $\{(\boldsymbol{m}_k, \boldsymbol{\Sigma}_k, a_k)\}_{k=1}^K$ and $\{(\boldsymbol{m}_l^\star, \boldsymbol{\Sigma}_l^\star, b_l)\}_{l=1}^L$) are then used to define objective in (16) for learning the graph filter. Once the graph filter $\mathbf{F}_G$ is optimized, its performance is evaluated on the test set.

During testing, for each test window $s = 1, \ldots, \mathcal{S} - 1$, the prediction is computed as $\widehat{f}_{\mathrm{test}}(V, \mathcal{T}_{s+1}) = \widetilde{\mathbf{F}}_G f_{\mathrm{test}}(V, \mathcal{T}_s)$, and the prediction error is evaluated using the relative squared error (RSE), defined by

$$\mathrm{RSE}^{(s)} = \frac{\|\widehat{f}_{\mathrm{test}}(V, \mathcal{T}_{s+1}) - f_{\mathrm{test}}(V, \mathcal{T}_s)\|_F^2}{\|f_{\mathrm{test}}(V, \mathcal{T}_s)\|_F^2}.$$

The final performance is measured by the mean of RSE across all prediction windows, defined as $\mathrm{MRSE} = \frac{1}{\mathcal{S}-1} \sum_{s=1}^{\mathcal{S}-1} \mathrm{RSE}^{(s)}$.

[1] https://github.com/nytimes/covid-19-data

2) Performance evaluation: We compare both *GDS-Cop* and *GDS-GMMs* against the following graph filtering learning methods for graph signal prediction:

a) **GSP-LS** (Least-Squares Graph Filtering) [2], [38]: The graph filter $\mathbf{F}_G$ is learned by minimizing the Frobenius norm of the difference between the filtered signals and the target signals, i.e., $\min_{\mathbf{F}_G} \|\mathbf{F}_G \mathbf{X} - \mathbf{X}^\star\|_F^2$.

b) **GSP-RLS** (Regularized Least-Squares Graph Filtering) [39], [40]: The graph filter $\mathbf{F}_G$ is learned by minimizing the same Frobenius norm objective as in GSP-LS, but with an additional ℓ_1-norm regularization term to promote sparsity in the filter coefficients, i.e., $\min_{\mathbf{F}_G} \|\mathbf{F}_G \mathbf{X} - \mathbf{X}^\star\|_F^2 + \lambda \|\mathbf{F}_G\|_1$, where $\lambda > 0$ controls the sparsity level.

c) **GSP-LSCM** (Least-Squares and Covariance-Matching Graph Filtering): This method extends GSP-LS by introducing a covariance-matching term into the objective. The graph filter $\mathbf{F}_G$ is learned by solving:

$$\min_{\mathbf{F}_G} \|\mathbf{F}_G \mathbf{X} - \mathbf{X}^\star\|_F^2 + \lambda \|\mathbf{F}_G \boldsymbol{\Sigma}_{\mathbf{X}} \mathbf{F}_G^\intercal - \boldsymbol{\Sigma}_{\mathbf{X}^\star}\|_F^2,$$

where $\boldsymbol{\Sigma}_{\mathbf{X}}$ and $\boldsymbol{\Sigma}_{\mathbf{X}^\star}$ are the empirical covariances of the input and target signals, respectively.

d) **GSP-LEV** (Log-Evidence Maximization with Heat Kernel Mixture) [41]: The graph filter is modeled as a convex combination of K heat diffusion kernels, i.e., $\mathbf{H}_G(\mathcal{T}) = \sum_{\tau \in \mathcal{T}} \pi^{(\tau)} \mathbf{H}_G(\tau)$ with $\mathbf{H}_G(\tau) = e^{-\tau \mathbf{L}_G}$, where $\mathcal{T}$ is a predefined set of diffusion scales and $\pi^{(\tau)} \ge 0$, $\sum_{\tau \in \mathcal{T}} \pi^{(\tau)} = 1$. The parameters π_τ, α and γ, are learned by maximizing the log-evidence:

$$\max_{\pi, \alpha, \gamma} \log \mathcal{N}\left(\mathbf{X}^\star \mid \mathbf{H}_G(\mathcal{T})\mathbf{X},\, \alpha^{-1}\mathbf{I} + \gamma^{-1}\mathbf{X}\mathbf{X}^\intercal\right).$$

For a fair comparison, the graph filter $\mathbf{F}_G$ is parameterized as a 2-order Chebyshev polynomial with three filter coefficients, i.e., $\mathbf{F}_G = \sum_{k=0}^2 \boldsymbol{\theta}_k T(\mathbf{L}_G)$, and this parameterization is used consistently across all methods, including GSP-LS, GSP-RLS, GSP-LSCM, and the proposed GDS-Cop and GDS-GMMs.

To verify that the GDS framework does not rely on complete observations or strict temporal correspondence, we consider two stress-test settings: *masking* and *shuffling*. In the masking setting, each graph signal (column) is partially observed through a Bernoulli mask, where the observation probability is randomly drawn from $[0.6, 0.9]$. Results are average over 10 random masks. As shown in Fig. 3a, GSP-LS, GSP-RLS, and GSP-LSCM degrade markedly due to their reliance on the complete observation assumption, while GSP-LEV, *GDS-Cop* and *GDS-GMMs* remain relatively robust since their distribution-matching formulations do not require full observations. In the shuffling setting, training data within each window is randomly permuted and results in Fig. 3b are averaged over 10 runs. From Fig. 3b, GSP-LS, GSP-RLS, and GSP-LSCM suffer worse accuracy because they depend on strict temporal alignment, whereas GSP-LEV, *GDS-Cop* and *GDS-GMMs* remain stable. This resilience highlights the advantage of the GDS framework in real-world scenarios with incomplete or misaligned data, since it models distributions of graph signals rather than individual temporally aligned observations.

This advantage is also evident in the window-size study in Fig. 3. Both *GDS-Cop* and *GDS-GMMs* achieve strong

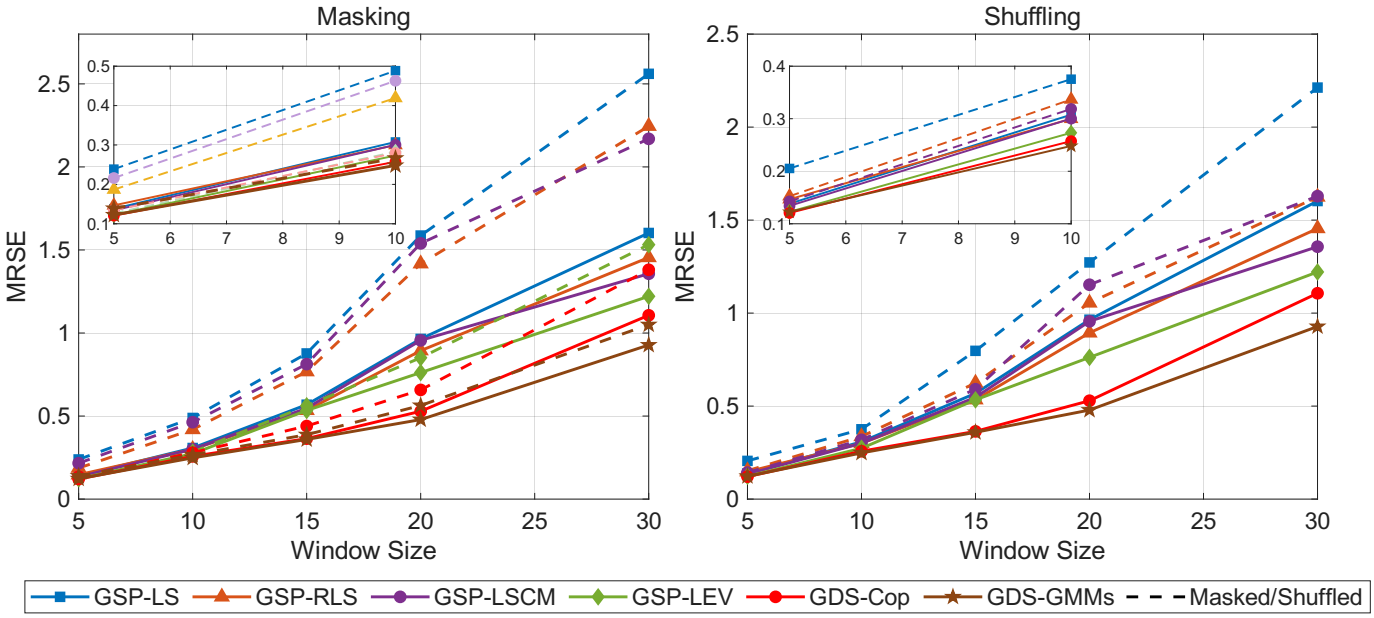

(a) Non-masking vs. Masking (b) Non-shuffling vs. Shuffling

Fig. 3. MRSE as a function of window size under masking and shuffling conditions. Solid lines represent the baseline setting, while dashed lines represent the masked and shuffled variants. Each method uses the same color for corresponding dashed and solid curves. Note that GDS-based methods are invariant to shuffling.

performance across all window sizes, with one of them attaining the lowest MRSE in each case. Their benefit becomes more pronounced for larger windows. In particular, *GDS-GMMs* tends to perform better when the window is large, likely because the increased number of samples allows more accurate estimation of the joint GMM. For smaller windows, *GDS-Cop* is slightly more reliable, suggesting greater robustness in low-sample regimes.

3) When is GSP approaches better?: We consider very small window sizes, namely $\mathcal{W} = 2, 3, 4$, with results reported in Table III. This regime is challenging for GDS-based methods because only a few samples are available within each window to estimate the underlying distribution, leading to less reliable GMM and copula estimates. Consequently, the performance advantage of GDS-based methods diminishes, and they underperform the GSP-based baselines in this small-sample regime. These results reveal a fundamental limitation of the proposed approach: its effectiveness depends critically on having a sufficient number of observations within each window to support reliable distribution estimation.

TABLE III
MRSE UNDER SMALL WINDOW SIZES

Window sizes	GSP-LS	GSP-RLS	GSP-LSCM	GDS-Cop	GDS-GMM
2	0.0487	0.0486	0.0412	0.0756	0.0943
3	0.0766	0.0762	0.0753	0.0959	0.1049
4	0.1065	0.1061	0.1040	0.1181	0.1095

B. Anomaly Detection

1) Dataset and experimental setup: We conduct anomaly detection experiments on a brain ECoG dataset,[2] consisting of normalized time-series recordings from 76 brain electrodes with 4000 time samples each, collected from an epilepsy patient during two seizure-related periods: pre-ictal (normal) and ictal (abnormal).

For each class, the ECoG time series is partitioned into non-overlapping segments of length 10, each modeled as a graph signal on a joint sensor-time graph $G = G_0 \times H$, where H is a path graph with 10 nodes (temporal dimension) and G_0 is a sensor graph over the 76 electrodes (spatial dimension). Thus G has 760 nodes indexed by (s, t), yielding 400 graph signals $\mathbf{x} \in \mathbb{R}^{760}$ per class, with joint Laplacian $\mathbf{L}_G = \mathbf{L}_H \otimes \mathbf{I}_{76} + \mathbf{I}_{10} \otimes \mathbf{L}_{G_0}$.

The sensor graph $G_0 \sim \nu_{\mathbf{x}}$ is constructed from the inter-electrode absolute correlation matrix. Given a batch of n signals, each signal is reshaped into a 76×10 electrode-time matrix, and the resulting $10n$ temporal samples are used to estimate the 76×76 pairwise correlations between electrodes. The graph G_0 is then obtained by thresholding this matrix at a random threshold $\rho \sim \mathcal{N}(\rho_0, \sigma_\rho^2)$ with $\rho_0 = 0.375$ and $\sigma_\rho^2 = 0.01$. As a practical instantiation of the SAGS, all signals within a batch share the same correlation structure, so $\nu_{\mathbf{x}}$ is constant within a batch, and its randomness arises from the stochastic threshold ρ. The signal-adaptive nature is reflected across batches: different batches correspond to different signal realizations, inducing different graph distributions, which is precisely what distinguishes normal from abnormal conditions in the spectral domain.

[2]https://math.bu.edu/people/kolaczyk/datasets.html

For each class, the 400 samples are split into $\mathcal{D}_{\text{train}}$, $\mathcal{D}_{\text{cal}}$, and $\mathcal{D}_{\text{test}}$ with ratio 2:1:1. We compute the GFT with respect to $\mathbf{L}_G$ and extract the high-frequency components in the spectral range $[\lambda_1, \lambda_2] = [730, 760]$, then aggregate them to estimate the class-specific reference distributions in (27). Fig. 4 visualizes the 4-component Gaussian mixture fits of the empirical high-frequency feature distributions for the two classes, which exhibit different peak locations in the frequency-feature space, motivating the peak location distance (28) as a discrepancy measure. During testing, each Monte Carlo run forms one test batch of n signals drawn from a single class, with normal and abnormal batches following a 2:1 ratio to reflect the class imbalance reported by NIHR, UK [42].

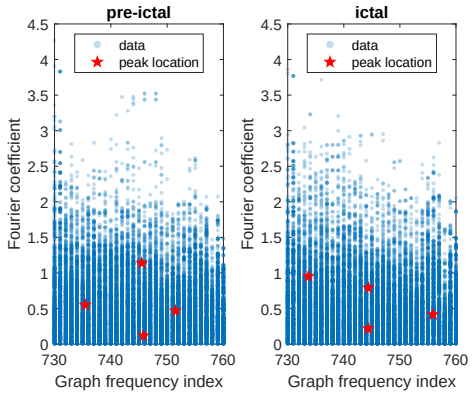

Fig. 4. Examples of Gaussian mixture fits of empirical distributions in the high-frequency domain. The peak locations can be used for detection.

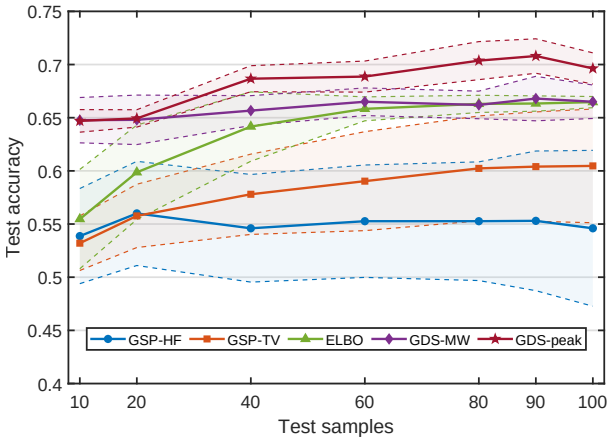

Fig. 5. Accuracy of anomaly detection w.r.t different sizes of test batch

2) Performance evaluation: We compare the proposed GDS-based approach, instantiated with two discrepancy measures, namely GDS-Peak (28) and GDS-MW (29), against the following baseline methods for graph signal anomaly detection:

a) **GSP-GFT** [37]: The classical GFT-based detector uses the batch-averaged maximum high-frequency coefficient magnitude $S_b = \frac{1}{n}\sum_{\mathbf{x}_m \in B_b} \max_{i\in\mathcal{I}} |(\mathbf{U}_{G_m}^{\intercal}\mathbf{x}_m)_i|$ as the test statistic, with threshold set as the average statistic over $\mathcal{D}_{\text{train}} \cup \mathcal{D}_{\text{cal}}$, and a test batch is declared abnormal if S_b exceeds it.

b) **GSP-TV** [43], [44]: The total-variation (TV) based detector exploits the smoothness of normal graph signals via the batch-averaged normalized Laplacian quadratic form $\text{TV}(B_b) = \frac{1}{n}\sum_{\mathbf{x}_m \in B_b} \mathbf{x}_m^{\intercal}\mathbf{L}_{G_m}\mathbf{x}_m / \|\mathbf{x}_m\|_2^2$. Batches from $\mathcal{D}_{\text{train}} \cup \mathcal{D}_{\text{cal}}$ provide the median TV m_0 and the quantile threshold τ; a test batch is declared abnormal if $|\text{TV}(B_b) - m_0| > \tau$.

c) **ELBO** [45], [46]: A variational autoencoder (VAE) [46] is trained on the high-frequency GFT coefficients of normal samples from $\mathcal{D}_{\text{train}}$, using the batch-averaged negative ELBO as the test statistic. The threshold τ is calibrated on $\mathcal{D}_{\text{cal}}$ via the $(1-\alpha)$-quantile, and a test batch is declared abnormal if its negative ELBO exceeds τ.

For all methods, detection performance is evaluated by the accuracy over N_{test} test batches,

$$\text{Acc} = \frac{1}{N_{\text{test}}}\sum_{b=1}^{N_{\text{test}}} \mathbf{1}[\hat{c}_b = c_b], \tag{30}$$

where c_b is the true label of the b-th test batch. We report Acc with respect to the test batch size (i.e, the number of test samples). For a fair comparison, the significance level is set to $\alpha = 0.05$ for all quantile-calibrated methods.

Fig. 5 reports the detection accuracy of all methods with respect to the test batch size n, from 10 to 100 in steps of 10. The two distribution-based methods, namely GDS-Peak and GDS-MW, consistently achieve the highest accuracy across all batch sizes and remain robust even with few test samples, since modeling the full distribution of high-frequency features captures distributional shifts that point-wise statistics miss. In contrast, the point-wise baselines are clearly limited: GSP-GFT, relying on a single high-frequency coefficient, plateaus at a low accuracy and barely improves with larger batches, confirming that a scalar statistic is insufficient to capture distributional differences; GSP-TV and ELBO improve as the batch size increases but require many more samples to approach, yet never surpass, the GDS methods. These results demonstrate that modeling the distributional structure of high-frequency components yields more reliable and sample-efficient anomaly detection.

VI. Conclusion

We propose a GDS framework that generalizes classical graph signal processing by modeling signals as probability distributions in the Wasserstein space and generalizing fixed graph topologies into signal-adaptive graph structures. This approach enables the principled handling of uncertainty and stochasticity in both signals and graphs, while strictly encompassing traditional GSP as a special case. We established a systematic correspondence between core GSP concepts and their GDS analogues, including the Fourier transform and filtering. Through two applications, graph filter learning and anomaly detection, we demonstrate the predictive benefits, robustness, and sample efficiency of the proposed framework. These results highlight the potential of the GDS framework for advancing GSP theory and for applications involving uncertain or irregular graph-structured data.

APPENDIX

A. Proof of Proposition 1

For any linear map $\mathbf{A} \in \mathbb{R}^{N\times N}$ and any coupling $\pi \in \Pi(\mu,\nu)$, the pushforward $(\mathbf{A},\mathbf{A})_*\pi$ is a coupling of $(\mathbf{A})_*\mu$ and $(\mathbf{A})_*\nu$. Therefore,

$$\begin{aligned} W_p^p((\mathbf{A})_*\mu,(\mathbf{A})_*\nu) &\le \int_{\mathbb{R}^N\times\mathbb{R}^N} \|\mathbf{A}\mathbf{x}-\mathbf{A}\mathbf{y}\|_2^p \,\mathrm{d}\pi(\mathbf{x},\mathbf{y}) \\ &\le \|\mathbf{A}\|_2^p \int_{\mathbb{R}^N\times\mathbb{R}^N} \|\mathbf{x}-\mathbf{y}\|_2^p \,\mathrm{d}\pi(\mathbf{x},\mathbf{y}). \end{aligned}$$

Taking the infimum over all $\pi \in \Pi(\mu,\nu)$ gives

$$W_p((\mathbf{A})_*\mu,(\mathbf{A})_*\nu) \le \|\mathbf{A}\|_2 W_p(\mu,\nu).$$

For Property (ii), since $\mathbf{U}_G$ is orthogonal, $\mathbf{U}_G^\intercal\mathbf{U}_G = \mathbf{I}$ and $\|\mathbf{U}_G^\intercal\mathbf{z}\|_2 = \|\mathbf{z}\|_2$ for every $\mathbf{z}\in\mathbb{R}^N$. Applying (6) with $\mathbf{A} = \mathbf{U}_G^\intercal$ yields

$$W_p((\mathbf{U}_G^\intercal)_*\mu,(\mathbf{U}_G^\intercal)_*\nu) \le W_p(\mu,\nu). \tag{31}$$

Conversely, applying the same inequality with $\mathbf{A} = \mathbf{U}_G$ to the transformed measures gives

$$\begin{aligned} W_p(\mu,\nu) &= W_p((\mathbf{U}_G)_*(\mathbf{U}_G^\intercal)_*\mu,\,(\mathbf{U}_G)_*(\mathbf{U}_G^\intercal)_*\nu) \\ &\le W_p((\mathbf{U}_G^\intercal)_*\mu,(\mathbf{U}_G^\intercal)_*\nu)\,. \end{aligned} \tag{32}$$

Combining (31) and (32) proves

$$W_p((\mathbf{U}_G^\intercal)_*\mu,(\mathbf{U}_G^\intercal)_*\nu) = W_p(\mu,\nu). \tag{33}$$

Property (iii) follows from the orthogonality of $\mathbf{U}_G$, which ensures that $(\mathbf{U}_G)_*(\mathbf{U}_G^\intercal)_*\mu = (\mathbf{U}_G\mathbf{U}_G^\intercal)_*\mu = \mu$. Property (iv) is a direct consequence of the composition rule for pushforward measures, namely $f_*(g_*\mu) = (f\circ g)_*\mu$, applied with $f = \mathbf{F}_G$ and $g = \mathbf{H}_G$.

B. Proof of Lemma 1

We begin by proving that $\mathcal{A}^*\mu$ is a probability measure on $\mathbb{R}^N\times\mathcal{G}_N$. Given a probability measure μ on $\mathbb{R}^N$ and a probability kernel $\nu_{\mathbf{x}}$ from $\mathbb{R}^N$ to $\mathcal{G}_N$, there exists a unique Borel probability measure on $\mathbb{R}^N\times\mathcal{G}_N$, namely the law of $(\mathbf{x},G)$ with $\mathbf{x}\sim\mu$ and $G \mid \mathbf{x}\sim\nu_{\mathbf{x}}$ [22, Sec. 4.1.3]. Setting $B = \mathcal{G}_N$ in (19) and using $\nu_{\mathbf{x}}(\mathcal{G}_N) = 1$ identifies the $\mathbb{R}^N$-marginal of $\mathcal{A}^*\mu$ as μ, i.e.,

$$(\mathcal{A}^*\mu)(A\times\mathcal{G}_N) = \int_A \nu_{\mathbf{x}}(\mathcal{G}_N)\,\mathrm{d}\mu(\mathbf{x}) = \mu(A).$$

with $A\in\mathcal{B}(\mathbb{R}^N)$.

Next, we verify that $\mathcal{A}^*\mu$ has finite p-th moment. Denote the metric $d_{\mathcal{G}}$ on $\mathcal{G}_N$ (i.e., the Euclidean metric induced by the adjacency parametrization) and equip $\mathbb{R}^N\times\mathcal{G}_N$ with

$$d_\times\big((\mathbf{x},G),(\mathbf{y},H)\big) := \big(\|\mathbf{x}-\mathbf{y}\|^p + d_{\mathcal{G}}(G,H)^p\big)^{1/p}.$$

Fix $z_0 = (\mathbf{0},G_0)$. For any $z = (\mathbf{x},G)\in\mathbb{R}^N\times\mathcal{G}_N$, we have

$$d_\times(z,z_0)^p = \|\mathbf{x}\|^p + d_{\mathcal{G}}(G,G_0)^p \ge 0.$$

Tonelli's theorem [22, Section 1.7] and the definition of $\mathcal{A}^*\mu$ yield

$$\begin{aligned} &\int_{\mathbb{R}^N\times\mathcal{G}_N} d_\times(z,z_0)^p\,\mathrm{d}(\mathcal{A}^*\mu)(z) \\ &\quad= \int_{\mathbb{R}^N}\int_{\mathcal{G}_N} (\|\mathbf{x}\|^p + d_{\mathcal{G}}(G,G_0)^p)\,\mathrm{d}\nu_{\mathbf{x}}(G)\,\mathrm{d}\mu(\mathbf{x}) \\ &\quad= \int_{\mathbb{R}^N}\|\mathbf{x}\|^p\,\mathrm{d}\mu(\mathbf{x}) + \int_{\mathbb{R}^N}\int_{\mathcal{G}_N} d_{\mathcal{G}}(G,G_0)^p\,\mathrm{d}\nu_{\mathbf{x}}(G)\,\mathrm{d}\mu(\mathbf{x}). \end{aligned}$$

The first term is finite since $\mu\in\mathcal{P}_p(\mathbb{R}^N)$. For the second term, since δ_{G_0} is the Dirac measure at G_0, the only coupling between $\nu_{\mathbf{x}}$ and δ_{G_0} is the product $\nu_{\mathbf{x}}\otimes\delta_{G_0}$. Hence, for every $\mathbf{x}\in\mathbb{R}^N$, $W_p^p(\nu_{\mathbf{x}},\delta_{G_0}) = \int_{\mathcal{G}_N} d_{\mathcal{G}}(G,G_0)^p\,\mathrm{d}\nu_{\mathbf{x}}(G)$. Therefore,

$$\begin{aligned} &\int_{\mathbb{R}^N}\int_{\mathcal{G}_N} d_{\mathcal{G}}(G,G_0)^p\,\mathrm{d}\nu_{\mathbf{x}}(G)\,\mathrm{d}\mu(\mathbf{x}) \\ &\quad= \int_{\mathbb{R}^N} W_p^p(\nu_{\mathbf{x}},\delta_{G_0})\,\mathrm{d}\mu(\mathbf{x}) < \infty, \end{aligned}$$

where the last inequality follows from (20). Combining this with the finiteness of the first term gives

$$\int_{\mathbb{R}^N\times\mathcal{G}_N} d_\times(z,z_0)^p\,\mathrm{d}(\mathcal{A}^*\mu)(z) < \infty.$$

Thus $\mathcal{A}^*\mu$ has finite p-th moment on $\mathbb{R}^N\times\mathcal{G}_N$. Since $\mathcal{A}^*\mu$ is a Borel probability measure on $\mathbb{R}^N\times\mathcal{G}_N$, we conclude that $\mathcal{A}^*\mu\in\mathcal{P}_p(\mathbb{R}^N\times\mathcal{G}_N)$.

C. Proof of Theorem 1

Since C is compact, every probability measure supported on C has finite p-th moment, and hence $\mathcal{P}(C) = \mathcal{P}_p(C)$. By Prokhorov's theorem [47] and the equivalence between weak convergence and W_p convergence on compact metric spaces, $\mathcal{P}(C)$ is compact under W_p. Since $\mathcal{M}: C\to\mathcal{P}_p(M_N(\mathbb{R}))$ is continuous and C is compact, the Heine-Cantor theorem implies that $\mathcal{M}$ is uniformly continuous on C. Define

$$R := \sup_{\mathbf{x}\in C}\|\mathbf{x}\| < \infty, \tag{34}$$

$$S := \sup_{\mathbf{x}\in C} W_p(\mathcal{M}(\mathbf{x}),\delta_{\mathbf{0}}) < \infty, \tag{35}$$

where $\delta_{\mathbf{0}}$ denotes the Dirac measure at the zero matrix in $M_N(\mathbb{R})$.

Step 1 (Dirac measures): We first show that the map $\mathbf{x}\mapsto\mathcal{T}(\delta_{\mathbf{x}})$ is uniformly continuous from C to $\mathcal{P}_p(\mathbb{R}^N)$. Fix $\mathbf{x}_1,\mathbf{x}_2\in C$. Let $\gamma_{\mathbf{x}_1,\mathbf{x}_2}$ be an optimal coupling between $\mathcal{M}(\mathbf{x}_1)$ and $\mathcal{M}(\mathbf{x}_2)$, i.e.,

$$\begin{aligned} &W_p^p(\mathcal{M}(\mathbf{x}_1),\mathcal{M}(\mathbf{x}_2)) \\ &\qquad= \int \|\mathbf{M}_1-\mathbf{M}_2\|^p\,\mathrm{d}\gamma_{\mathbf{x}_1,\mathbf{x}_2}(\mathbf{M}_1,\mathbf{M}_2). \end{aligned} \tag{36}$$

Since $\mathcal{M}$ is continuous on the compact set C, the map $(\mathbf{x}_1,\mathbf{x}_2)\mapsto(\mathcal{M}(\mathbf{x}_1),\mathcal{M}(\mathbf{x}_2))$ is continuous, hence Borel measurable, from $C\times C$ to $\mathcal{P}_p(M_N(\mathbb{R}))\times\mathcal{P}_p(M_N(\mathbb{R}))$. By the measurable selection theorem for optimal couplings [20, Corollary 5.22], the fiberwise optimal couplings can be chosen so that $(\mathbf{x}_1,\mathbf{x}_2)\mapsto\gamma_{\mathbf{x}_1,\mathbf{x}_2}$ is a Borel-measurable kernel from $C\times C$ to $\mathcal{P}\big(M_N(\mathbb{R})\times M_N(\mathbb{R})\big)$; we fix such a

measurable selection throughout. Push $\gamma_{\mathbf{x}_1,\mathbf{x}_2}$ forward through the map $(\mathbf{M}_1,\mathbf{M}_2)\mapsto(\mathbf{M}_1\mathbf{x}_1,\mathbf{M}_2\mathbf{x}_2)$ and denote the resulting measure on $\mathbb{R}^N\times\mathbb{R}^N$ by $\gamma'_{\mathbf{x}_1,\mathbf{x}_2}$. By construction, $\gamma'_{\mathbf{x}_1,\mathbf{x}_2}$ is a coupling between $\mathcal{T}(\delta_{\mathbf{x}_1})$ and $\mathcal{T}(\delta_{\mathbf{x}_2})$, and, since pushforward under a fixed continuous map preserves measurability of kernels, $(\mathbf{x}_1,\mathbf{x}_2)\mapsto\gamma'_{\mathbf{x}_1,\mathbf{x}_2}$ is likewise a Borel-measurable kernel on $C\times C$. Hence,

$$\begin{aligned}&W_p^p(\mathcal{T}(\delta_{\mathbf{x}_1}),\mathcal{T}(\delta_{\mathbf{x}_2}))\\&\quad\le\int\|\mathbf{M}_1\mathbf{x}_1-\mathbf{M}_2\mathbf{x}_2\|^p\,\mathrm{d}\gamma_{\mathbf{x}_1,\mathbf{x}_2}(\mathbf{M}_1,\mathbf{M}_2).\end{aligned}\tag{37}$$

Using $\mathbf{M}_1\mathbf{x}_1-\mathbf{M}_2\mathbf{x}_2=(\mathbf{M}_1-\mathbf{M}_2)\mathbf{x}_1+\mathbf{M}_2(\mathbf{x}_1-\mathbf{x}_2)$ and $\|a+b\|^p\le 2^{p-1}(\|a\|^p+\|b\|^p)$, we obtain

$$\begin{aligned}W_p^p(\mathcal{T}(\delta_{\mathbf{x}_1}),\mathcal{T}(\delta_{\mathbf{x}_2}))\le 2^{p-1}&\int\|(\mathbf{M}_1-\mathbf{M}_2)\mathbf{x}_1\|^p\,\mathrm{d}\gamma_{\mathbf{x}_1,\mathbf{x}_2}\\&+2^{p-1}\int\|\mathbf{M}_2(\mathbf{x}_1-\mathbf{x}_2)\|^p\,\mathrm{d}\gamma_{\mathbf{x}_1,\mathbf{x}_2}.\end{aligned}\tag{38}$$

The first term on the right-hand side (R.H.S.) of (38) is bounded as:

$$\int\|(\mathbf{M}_1-\mathbf{M}_2)\mathbf{x}_1\|^p\,\mathrm{d}\gamma_{\mathbf{x}_1,\mathbf{x}_2}\le R^pW_p^p(\mathcal{M}(\mathbf{x}_1),\mathcal{M}(\mathbf{x}_2)).\tag{39}$$

For the second term, using $\|\mathbf{M}_2(\mathbf{x}_1-\mathbf{x}_2)\|\le\|\mathbf{M}_2\|\|\mathbf{x}_1-\mathbf{x}_2\|$ and noting that the second marginal of $\gamma_{\mathbf{x}_1,\mathbf{x}_2}$ is $\mathcal{M}(\mathbf{x}_2)$, we have

$$\begin{aligned}&\int\|\mathbf{M}_2(\mathbf{x}_1-\mathbf{x}_2)\|^p\,\mathrm{d}\gamma_{\mathbf{x}_1,\mathbf{x}_2}\\&\le\|\mathbf{x}_1-\mathbf{x}_2\|^p\int\|\mathbf{M}_2\|^p\,\mathrm{d}\mathcal{M}(\mathbf{x}_2)(\mathbf{M}_2)\\&=\|\mathbf{x}_1-\mathbf{x}_2\|^pW_p^p(\mathcal{M}(\mathbf{x}_2),\delta_{\mathbf{0}})\\&\le S^p\|\mathbf{x}_1-\mathbf{x}_2\|^p.\end{aligned}\tag{40}$$

Combining (37), (39) and (40), we arrive at

$$\begin{aligned}W_p^p(\mathcal{T}(\delta_{\mathbf{x}_1}),\mathcal{T}(\delta_{\mathbf{x}_2}))\le{}&2^{p-1}R^pW_p^p(\mathcal{M}(\mathbf{x}_1),\mathcal{M}(\mathbf{x}_2))\\&+2^{p-1}S^p\|\mathbf{x}_1-\mathbf{x}_2\|^p.\end{aligned}\tag{41}$$

Since $\mathcal{M}$ is uniformly continuous on C, both terms on the R.H.S. converge to zero uniformly as $\|\mathbf{x}_1-\mathbf{x}_2\|\to 0$. Hence, $\mathbf{x}\mapsto\mathcal{T}(\delta_{\mathbf{x}})$ is uniformly continuous on C.

Step 2 (General measures): Let $\mu,\mu'\in\mathcal{P}(C)$. Let η be an optimal coupling between μ and μ'. Thus,

$$W_p^p(\mu,\mu')=\int_{C\times C}\|\mathbf{x}_1-\mathbf{x}_2\|^p\,\mathrm{d}\eta(\mathbf{x}_1,\mathbf{x}_2).\tag{42}$$

For each $(\mathbf{x}_1,\mathbf{x}_2)\in C\times C$, let $\gamma'_{\mathbf{x}_1,\mathbf{x}_2}$ be the coupling between $\mathcal{T}(\delta_{\mathbf{x}_1})$ and $\mathcal{T}(\delta_{\mathbf{x}_2})$ constructed in *Step 1*, i.e. $\gamma'_{\mathbf{x}_1,\mathbf{x}_2}$ is obtained by pushing forward $\gamma_{\mathbf{x}_1,\mathbf{x}_2}$ through the map $(\mathbf{M}_1,\mathbf{M}_2)\mapsto(\mathbf{M}_1\mathbf{x}_1,\mathbf{M}_2\mathbf{x}_2)$, using the Borel-measurable kernel $(\mathbf{x}_1,\mathbf{x}_2)\mapsto\gamma_{\mathbf{x}_1,\mathbf{x}_2}$ fixed in *Step 1*. Define a measure η' on $\mathbb{R}^N\times\mathbb{R}^N$ by requiring that, for every bounded continuous function $g:\mathbb{R}^N\times\mathbb{R}^N\to\mathbb{R}$,

$$\begin{aligned}&\int_{\mathbb{R}^N\times\mathbb{R}^N}g(\mathbf{w}_1,\mathbf{w}_2)\,\mathrm{d}\eta'(\mathbf{w}_1,\mathbf{w}_2)\\&:=\int_{C\times C}\int_{\mathbb{R}^N\times\mathbb{R}^N}g(\mathbf{w}_1,\mathbf{w}_2)\,\mathrm{d}\gamma'_{\mathbf{x}_1,\mathbf{x}_2}(\mathbf{w}_1,\mathbf{w}_2)\,\mathrm{d}\eta(\mathbf{x}_1,\mathbf{x}_2).\end{aligned}\tag{43}$$

This is well defined since $(\mathbf{x}_1,\mathbf{x}_2)\mapsto\gamma'_{\mathbf{x}_1,\mathbf{x}_2}$ is a Borel-measurable kernel and g is bounded and continuous, the map $(\mathbf{x}_1,\mathbf{x}_2)\mapsto\int g\,d\gamma'_{\mathbf{x}_1,\mathbf{x}_2}$ is Borel measurable and bounded on the compact set $C\times C$. Therefore, the outer integral against η is well defined; the resulting functional $g\mapsto\int g\,d\eta'$ is positive and linear on bounded continuous functions with $\int\mathrm{d}\eta'=1$, so by the Riesz representation theorem it defines a (unique) Borel probability measure η' on $\mathbb{R}^N\times\mathbb{R}^N$. We now verify that η' is a coupling between $\mathcal{T}(\mu)$ and $\mathcal{T}(\mu')$. Let $h:\mathbb{R}^N\to\mathbb{R}$ be bounded and continuous. Since the first marginal of $\gamma'_{\mathbf{x}_1,\mathbf{x}_2}$ is $\mathcal{T}(\delta_{\mathbf{x}_1})$, we have

$$\begin{aligned}&\int_{\mathbb{R}^N\times\mathbb{R}^N}h(\mathbf{w}_1)\,\mathrm{d}\eta'(\mathbf{w}_1,\mathbf{w}_2)\\&=\int_{C\times C}\int_{\mathbb{R}^N\times\mathbb{R}^N}h(\mathbf{w}_1)\,\mathrm{d}\gamma'_{\mathbf{x}_1,\mathbf{x}_2}(\mathbf{w}_1,\mathbf{w}_2)\,\mathrm{d}\eta(\mathbf{x}_1,\mathbf{x}_2)\\&=\int_{C\times C}\int_{\mathbb{R}^N}h(\mathbf{w}_1)\,\mathrm{d}\mathcal{T}(\delta_{\mathbf{x}_1})(\mathbf{w}_1)\,\mathrm{d}\eta(\mathbf{x}_1,\mathbf{x}_2)\\&=\int_C\int_{\mathbb{R}^N}h(\mathbf{w}_1)\,\mathrm{d}\mathcal{T}(\delta_{\mathbf{x}_1})(\mathbf{w}_1)\,\mathrm{d}\mu(\mathbf{x}_1)\\&=\int_{\mathbb{R}^N}h(\mathbf{w}_1)\,\mathrm{d}\mathcal{T}(\mu)(\mathbf{w}_1).\end{aligned}\tag{44}$$

Thus the first marginal of η' is $\mathcal{T}(\mu)$. By the same argument, the second marginal of η' is $\mathcal{T}(\mu')$. Since η' is a coupling between $\mathcal{T}(\mu)$ and $\mathcal{T}(\mu')$,

$$\begin{aligned}W_p^p(\mathcal{T}(\mu),\mathcal{T}(\mu'))&\le\int_{\mathbb{R}^N\times\mathbb{R}^N}\|\mathbf{w}_1-\mathbf{w}_2\|^p\,\mathrm{d}\eta'(\mathbf{w}_1,\mathbf{w}_2)\\&=\int_{C\times C}\int_{\mathbb{R}^N\times\mathbb{R}^N}\|\mathbf{w}_1-\mathbf{w}_2\|^p\,\mathrm{d}\gamma'_{\mathbf{x}_1,\mathbf{x}_2}(\mathbf{w}_1,\mathbf{w}_2)\,\mathrm{d}\eta(\mathbf{x}_1,\mathbf{x}_2)\end{aligned}\tag{45}$$

Let $\omega(r):=\sup_{\substack{\mathbf{x}_1,\mathbf{x}_2\in C\\\|\mathbf{x}_1-\mathbf{x}_2\|\le r}}W_p\left(\mathcal{M}(\mathbf{x}_1),\mathcal{M}(\mathbf{x}_2)\right)$. Since $\mathcal{M}$ is uniformly continuous on C, we have $\omega(r)\to 0$ as $r\to 0$. Moreover, by the estimate in *Step 1*, the inner integral satisfies

$$\begin{aligned}&\int_{\mathbb{R}^N\times\mathbb{R}^N}\|\mathbf{w}_1-\mathbf{w}_2\|^p\,\mathrm{d}\gamma'_{\mathbf{x}_1,\mathbf{x}_2}(\mathbf{w}_1,\mathbf{w}_2)\\&\le 2^{p-1}R^pW_p^p(\mathcal{M}(\mathbf{x}_1),\mathcal{M}(\mathbf{x}_2))+2^{p-1}S^p\|\mathbf{x}_1-\mathbf{x}_2\|^p.\end{aligned}$$

Fix $\varepsilon>0$. Split the integral over $C\times C$ into the regions $\|\mathbf{x}_1-\mathbf{x}_2\|<\varepsilon$ and $\|\mathbf{x}_1-\mathbf{x}_2\|\ge\varepsilon$. On the first region, we have $W_p^p(\mathcal{M}(\mathbf{x}_1),\mathcal{M}(\mathbf{x}_2))\le\omega(\varepsilon)^p$. On the second region, using the triangle inequality and the definition of S in (34), we have

$$\begin{aligned}&W_p(\mathcal{M}(\mathbf{x}_1),\mathcal{M}(\mathbf{x}_2))\\&\le W_p(\mathcal{M}(\mathbf{x}_1),\delta_{\mathbf{0}})+W_p(\mathcal{M}(\mathbf{x}_2),\delta_{\mathbf{0}})\le 2S,\end{aligned}$$

so that

$$W_p^p(\mathcal{M}(\mathbf{x}_1),\mathcal{M}(\mathbf{x}_2))\le(2S)^p.$$

Moreover, by Markov's inequality, we have

$$\begin{aligned}&\eta(\|\mathbf{x}_1-\mathbf{x}_2\|\ge\varepsilon)\\&\quad\le\frac{1}{\varepsilon^p}\int_{C\times C}\|\mathbf{x}_1-\mathbf{x}_2\|^p\,\mathrm{d}\eta(\mathbf{x}_1,\mathbf{x}_2)=\frac{W_p^p(\mu,\mu')}{\varepsilon^p}\end{aligned}$$

where the last equality follows from the optimality of the coupling η. Therefore,

$$W_p^p(\mathcal{T}(\mu),\mathcal{T}(\mu')) \le 2^{p-1}R^p\omega(\varepsilon)^p + 2^{p-1}R^p(2S)^p\frac{W_p^p(\mu,\mu')}{\varepsilon^p} + 2^{p-1}S^pW_p^p(\mu,\mu').$$

Given any $\alpha > 0$, choose $\varepsilon > 0$ sufficiently small such that $2^{p-1}R^p\omega(\varepsilon)^p < \alpha^p/2$. For this fixed ε, define $B_\varepsilon := 2^{p-1}R^p(2S)^p/\varepsilon^p + 2^{p-1}S^p$. Choose $\kappa := (\alpha^p/(2B_\varepsilon))^{1/p}$. Then, for all $\mu,\mu' \in \mathcal{P}_p(C)$ satisfying $W_p(\mu,\mu') < \kappa$, we have

$$\begin{aligned} W_p^p(\mathcal{T}(\mu),\mathcal{T}(\mu')) &< 2^{p-1}R^p\omega(\varepsilon)^p + B_\varepsilon W_p^p(\mu,\mu') \\ &< \frac{\alpha^p}{2} + B_\varepsilon\kappa^p = \frac{\alpha^p}{2} + \frac{\alpha^p}{2} = \alpha^p. \end{aligned} \tag{46}$$

Since κ depends only on α and not on the particular μ and μ', this proves that $\mathcal{T} : \mathcal{P}_p(C) \to \mathcal{P}_p(\mathbb{R}^N)$ is uniformly continuous.

D. Proof of Theorem 2

Let $L > 0$ be the Lipschitz constant of $\mathcal{M}$, and let $\delta_{\mathbf{0}}$ denote the Dirac measure at the zero matrix in $M_N(\mathbb{R})$. Since $\mathcal{M}(\mathbf{0}) \in \mathcal{P}_p(M_N(\mathbb{R}))$, define

$$S_0 := W_p(\mathcal{M}(\mathbf{0}),\delta_{\mathbf{0}}) < \infty.$$

By the triangle inequality and the Lipschitz continuity of $\mathcal{M}$, for every $\mathbf{x} \in \mathbb{R}^N$, we have

$$\begin{aligned} W_p(\mathcal{M}(\mathbf{x}),\delta_{\mathbf{0}}) &\le W_p(\mathcal{M}(\mathbf{x}),\mathcal{M}(\mathbf{0})) + W_p(\mathcal{M}(\mathbf{0}),\delta_{\mathbf{0}}) \\ &\le L\|\mathbf{x}\| + S_0 \end{aligned} \tag{47}$$

We first verify that $\mathcal{T}(\mu) \in \mathcal{P}_p(\mathbb{R}^N)$ for every $\mu \in \mathcal{P}_{2p}(\mathbb{R}^N)$. Let $\mu \in \mathcal{P}_{2p}(\mathbb{R}^N)$. Since $\mathcal{T}(\mu)$ is the distribution of $\mathbf{w} = \mathbf{M}\mathbf{x}$, where $\mathbf{x} \sim \mu$ and $\mathbf{M} \sim \mathcal{M}(\mathbf{x})$, we have

$$\begin{aligned} &\int_{\mathbb{R}^N} \|\mathbf{w}\|^p \,\mathrm{d}\mathcal{T}(\mu)(\mathbf{w}) \\ &\quad= \int_{\mathbb{R}^N}\int_{M_N(\mathbb{R})} \|\mathbf{M}\mathbf{x}\|^p \,\mathrm{d}\mathcal{M}(\mathbf{x})(\mathbf{M})\,\mathrm{d}\mu(\mathbf{x}) \\ &\quad\le \int_{\mathbb{R}^N} \|\mathbf{x}\|^p \int_{M_N(\mathbb{R})} \|\mathbf{M}\|^p \,\mathrm{d}\mathcal{M}(\mathbf{x})(\mathbf{M})\,\mathrm{d}\mu(\mathbf{x}) \\ &\quad= \int_{\mathbb{R}^N} \|\mathbf{x}\|^p W_p^p\big(\mathcal{M}(\mathbf{x}),\delta_{\mathbf{0}}\big)\,\mathrm{d}\mu(\mathbf{x}) \\ &\quad\le \int_{\mathbb{R}^N} \|\mathbf{x}\|^p \big(L\|\mathbf{x}\| + S_0\big)^p \,\mathrm{d}\mu(\mathbf{x}). \end{aligned} \tag{48}$$

Moreover,

$$\|\mathbf{x}\|^p\big(L\|\mathbf{x}\| + S_0\big)^p \le 2^{p-1}L^p\|\mathbf{x}\|^{2p} + 2^{p-1}S_0^p\|\mathbf{x}\|^p.$$

Since $\mu \in \mathcal{P}_{2p}(\mathbb{R}^N)$, the right-hand side of (48) is finite. Hence, $\mathcal{T}(\mu) \in \mathcal{P}_p(\mathbb{R}^N)$. Therefore, $\mathcal{T}$ is well-defined on $\mathcal{P}_{2p}(\mathbb{R}^N)$.

We now prove continuity at an arbitrary $\mu \in \mathcal{P}_{2p}(\mathbb{R}^N)$. Let $\mu' \in \mathcal{P}_{2p}(\mathbb{R}^N)$, and let η be an optimal coupling between μ and μ' for W_{2p}. Then,

$$W_{2p}(\mu,\mu') = \left(\int_{\mathbb{R}^N\times\mathbb{R}^N} \|\mathbf{x}_1 - \mathbf{x}_2\|^{2p}\,\mathrm{d}\eta(\mathbf{x}_1,\mathbf{x}_2)\right)^{\frac{1}{2p}}. \tag{49}$$

For each pair $(\mathbf{x}_1,\mathbf{x}_2)$, let $\gamma_{\mathbf{x}_1,\mathbf{x}_2}$ be an optimal coupling between $\mathcal{M}(\mathbf{x}_1)$ and $\mathcal{M}(\mathbf{x}_2)$. Since $\mathcal{M}$ is Lipschitz continuous, it is in particular Borel measurable from $\mathbb{R}^N$ to $\mathcal{P}_p(M_N(\mathbb{R}))$. Using the same argument as in the proof of Theorem 1, we can fix a Borel-measurable kernel $(\mathbf{x}_1,\mathbf{x}_2) \mapsto \gamma_{\mathbf{x}_1,\mathbf{x}_2}$ from $\mathbb{R}^N \times \mathbb{R}^N$ to $\mathcal{P}(M_N(\mathbb{R}) \times M_N(\mathbb{R}))$ such that $\gamma_{\mathbf{x}_1,\mathbf{x}_2}$ is optimal between $\mathcal{M}(\mathbf{x}_1)$ and $\mathcal{M}(\mathbf{x}_2)$ for every $(\mathbf{x}_1,\mathbf{x}_2)$. Push it forward through the map

$$(\mathbf{M}_1,\mathbf{M}_2) \mapsto (\mathbf{M}_1\mathbf{x}_1, \mathbf{M}_2\mathbf{x}_2),$$

and denote the resulting coupling between $\mathcal{T}(\delta_{\mathbf{x}_1})$ and $\mathcal{T}(\delta_{\mathbf{x}_2})$ by $\gamma'_{\mathbf{x}_1,\mathbf{x}_2}$. Since pushforward under a fixed continuous map preserves measurability of kernels, $(\mathbf{x}_1,\mathbf{x}_2) \mapsto \gamma'_{\mathbf{x}_1,\mathbf{x}_2}$ is likewise a Borel-measurable kernel. Define the corresponding fiberwise cost

$$Q_p(\mathbf{x}_1,\mathbf{x}_2) := \int_{\mathbb{R}^N\times\mathbb{R}^N} \|\mathbf{w}_1 - \mathbf{w}_2\|^p \,\mathrm{d}\gamma'_{\mathbf{x}_1,\mathbf{x}_2}(\mathbf{w}_1,\mathbf{w}_2).$$

By construction,

$$\begin{aligned} &Q_p(\mathbf{x}_1,\mathbf{x}_2) \\ &\quad= \int_{M_N(\mathbb{R})\times M_N(\mathbb{R})} \|\mathbf{M}_1\mathbf{x}_1 - \mathbf{M}_2\mathbf{x}_2\|^p \,\mathrm{d}\gamma_{\mathbf{x}_1,\mathbf{x}_2}(\mathbf{M}_1,\mathbf{M}_2). \end{aligned}$$

Using the decomposition

$$\mathbf{M}_1\mathbf{x}_1 - \mathbf{M}_2\mathbf{x}_2 = (\mathbf{M}_1 - \mathbf{M}_2)\mathbf{x}_1 + \mathbf{M}_2(\mathbf{x}_1 - \mathbf{x}_2)$$

and the triangle inequality

$$\|a+b\|^p \le 2^{p-1}\big(\|a\|^p + \|b\|^p\big),$$

we obtain

$$\begin{aligned} &Q_p(\mathbf{x}_1,\mathbf{x}_2) \\ &\quad\le 2^{p-1}\int_{M_N(\mathbb{R})\times M_N(\mathbb{R})} \|(\mathbf{M}_1 - \mathbf{M}_2)\mathbf{x}_1\|^p \,\mathrm{d}\gamma_{\mathbf{x}_1,\mathbf{x}_2} \\ &\qquad+ 2^{p-1}\int_{M_N(\mathbb{R})\times M_N(\mathbb{R})} \|\mathbf{M}_2(\mathbf{x}_1 - \mathbf{x}_2)\|^p \,\mathrm{d}\gamma_{\mathbf{x}_1,\mathbf{x}_2}. \end{aligned} \tag{50}$$

For the first term, since

$$\|(\mathbf{M}_1 - \mathbf{M}_2)\mathbf{x}_1\| \le \|\mathbf{M}_1 - \mathbf{M}_2\|_{\mathrm{op}}\|\mathbf{x}_1\|,$$

and $\gamma_{\mathbf{x}_1,\mathbf{x}_2}$ is optimal between $\mathcal{M}(\mathbf{x}_1)$ and $\mathcal{M}(\mathbf{x}_2)$, we have

$$\begin{aligned} &\int_{M_N(\mathbb{R})\times M_N(\mathbb{R})} \|(\mathbf{M}_1 - \mathbf{M}_2)\mathbf{x}_1\|^p \,\mathrm{d}\gamma_{\mathbf{x}_1,\mathbf{x}_2} \\ &\qquad\le \|\mathbf{x}_1\|^p W_p^p\big(\mathcal{M}(\mathbf{x}_1),\mathcal{M}(\mathbf{x}_2)\big) \\ &\qquad\le L^p\|\mathbf{x}_1\|^p\|\mathbf{x}_1 - \mathbf{x}_2\|^p. \end{aligned} \tag{51}$$

For the second term, since

$$\|\mathbf{M}_2(\mathbf{x}_1 - \mathbf{x}_2)\| \le \|\mathbf{M}_2\|_{\mathrm{op}}\|\mathbf{x}_1 - \mathbf{x}_2\|,$$

and the second marginal of $\gamma_{\mathbf{x}_1,\mathbf{x}_2}$ is $\mathcal{M}(\mathbf{x}_2)$, we obtain

$$\begin{aligned} &\int_{M_N(\mathbb{R})\times M_N(\mathbb{R})} \|\mathbf{M}_2(\mathbf{x}_1 - \mathbf{x}_2)\|^p \,\mathrm{d}\gamma_{\mathbf{x}_1,\mathbf{x}_2} \\ &\qquad\le \|\mathbf{x}_1 - \mathbf{x}_2\|^p W_p^p\big(\mathcal{M}(\mathbf{x}_2),\delta_{\mathbf{0}}\big) \\ &\qquad\le \big(L\|\mathbf{x}_2\| + S_0\big)^p\|\mathbf{x}_1 - \mathbf{x}_2\|^p, \end{aligned} \tag{52}$$

where the last inequality follows from (47). Combining (50) to (52), we get

$$\begin{aligned} &Q_p(\mathbf{x}_1,\mathbf{x}_2) \\ &\quad\le 2^{p-1}\Big[L^p\|\mathbf{x}_1\|^p + \big(L\|\mathbf{x}_2\|+S_0\big)^p\Big]\|\mathbf{x}_1-\mathbf{x}_2\|^p. \end{aligned} \tag{53}$$

Next, because $(\mathbf{x}_1,\mathbf{x}_2)\mapsto\gamma'_{\mathbf{x}_1,\mathbf{x}_2}$ is a Borel-measurable kernel, we may define a measure η' on $\mathbb{R}^N\times\mathbb{R}^N$ via the disintegration formula: for any Borel set $A\subseteq\mathbb{R}^N\times\mathbb{R}^N$,

$$\eta'(A) := \int_{\mathbb{R}^N\times\mathbb{R}^N}\gamma'_{\mathbf{x}_1,\mathbf{x}_2}(A)\;\mathrm{d}\eta(\mathbf{x}_1,\mathbf{x}_2),$$

i.e., η' is obtained by first sampling $(\mathbf{x}_1,\mathbf{x}_2)\sim\eta$ and then sampling $(\mathbf{w}_1,\mathbf{w}_2)\sim\gamma'_{\mathbf{x}_1,\mathbf{x}_2}$. Since the first marginal of $\gamma'_{\mathbf{x}_1,\mathbf{x}_2}$ equals $\mathcal{T}(\delta_{\mathbf{x}_1})$ for every $\mathbf{x}_1$, and the first marginal of η is μ, integrating over $\mathbf{x}_1\sim\mu$ shows that the first marginal of η' is $\int\mathcal{T}(\delta_{\mathbf{x}_1})\;\mathrm{d}\mu(\mathbf{x}_1)=\mathcal{T}(\mu)$; by the symmetric argument, the second marginal of η' is $\mathcal{T}(\mu')$. Hence η' is a valid coupling of $\mathcal{T}(\mu)$ and $\mathcal{T}(\mu')$. Moreover, since $\|\mathbf{w}_1-\mathbf{w}_2\|^p\ge 0$, Tonelli's theorem gives

$$\begin{aligned} &\int_{\mathbb{R}^N\times\mathbb{R}^N}\|\mathbf{w}_1-\mathbf{w}_2\|^p\;\mathrm{d}\eta'(\mathbf{w}_1,\mathbf{w}_2) \\ &\quad=\int_{\mathbb{R}^N\times\mathbb{R}^N}Q_p(\mathbf{x}_1,\mathbf{x}_2)\;\mathrm{d}\eta(\mathbf{x}_1,\mathbf{x}_2). \end{aligned}$$

Since η' is a coupling of $\mathcal{T}(\mu)$ and $\mathcal{T}(\mu')$, we conclude

$$W_p^p\big(\mathcal{T}(\mu),\mathcal{T}(\mu')\big)\le\int_{\mathbb{R}^N\times\mathbb{R}^N}Q_p(\mathbf{x}_1,\mathbf{x}_2)\;\mathrm{d}\eta(\mathbf{x}_1,\mathbf{x}_2).$$

Using (53), this gives

$$\begin{aligned} &W_p^p\big(\mathcal{T}(\mu),\mathcal{T}(\mu')\big) \\ &\quad\le 2^{p-1}L^p\int\|\mathbf{x}_1\|^p\|\mathbf{x}_1-\mathbf{x}_2\|^p\;\mathrm{d}\eta \\ &\qquad+2^{p-1}\int\big(L\|\mathbf{x}_2\|+S_0\big)^p\|\mathbf{x}_1-\mathbf{x}_2\|^p\;\mathrm{d}\eta. \end{aligned} \tag{54}$$

By Hölder's inequality,

$$\begin{aligned} &\int\|\mathbf{x}_1\|^p\|\mathbf{x}_1-\mathbf{x}_2\|^p\;\mathrm{d}\eta \\ &\quad\le\left(\int\|\mathbf{x}_1\|^{2p}\;\mathrm{d}\eta\right)^{1/2}\left(\int\|\mathbf{x}_1-\mathbf{x}_2\|^{2p}\;\mathrm{d}\eta\right)^{1/2} \\ &\quad=W_{2p}^p(\mu,\delta_{\mathbf{0}})W_{2p}^p(\mu,\mu'). \end{aligned} \tag{55}$$

Similarly,

$$\begin{aligned} &\int\big(L\|\mathbf{x}_2\|+S_0\big)^p\|\mathbf{x}_1-\mathbf{x}_2\|^p\;\mathrm{d}\eta \\ &\quad\le\left(\int\big(L\|\mathbf{x}_2\|+S_0\big)^{2p}\;\mathrm{d}\eta\right)^{1/2}\left(\int\|\mathbf{x}_1-\mathbf{x}_2\|^{2p}\;\mathrm{d}\eta\right)^{1/2} \\ &\quad=\left(\int_{\mathbb{R}^N}\big(L\|\mathbf{x}\|+S_0\big)^{2p}\;\mathrm{d}\mu'(\mathbf{x})\right)^{1/2}W_{2p}^p(\mu,\mu'). \end{aligned} \tag{56}$$

Substituting (55) and (56) into (54), we obtain

$$W_p^p\big(\mathcal{T}(\mu),\mathcal{T}(\mu')\big)\le C(\mu,\mu')W_{2p}^p(\mu,\mu'),$$

where

$$\begin{aligned} C(\mu,\mu') :&= 2^{p-1}L^pW_{2p}^p(\mu,\delta_{\mathbf{0}}) \\ &\quad+2^{p-1}\left(\int_{\mathbb{R}^N}\big(L\|\mathbf{x}\|+S_0\big)^{2p}\;\mathrm{d}\mu'(\mathbf{x})\right)^{1/2}. \end{aligned} \tag{57}$$

Now fix $\mu\in\mathcal{P}_{2p}(\mathbb{R}^N)$, and let $r>0$ be arbitrary. If $W_{2p}(\mu,\mu')\le r$, then by the triangle inequality, we have

$$W_{2p}(\mu',\delta_{\mathbf{0}})\le W_{2p}(\mu',\mu)+W_{2p}(\mu,\delta_{\mathbf{0}})\le r+W_{2p}(\mu,\delta_{\mathbf{0}}).$$

Hence the $2p$-th moments of all μ' satisfying $W_{2p}(\mu,\mu')\le r$ are uniformly bounded. In particular,

$$\left(\int_{\mathbb{R}^N}\big(L\|\mathbf{x}\|+S_0\big)^{2p}\;\mathrm{d}\mu'(\mathbf{x})\right)^{1/2}$$

is uniformly bounded over the W_{2p}-ball

$$\{\mu'\in\mathcal{P}_{2p}(\mathbb{R}^N):W_{2p}(\mu,\mu')\le r\}.$$

Therefore, there exists a finite constant $C_{\mu,r}>0$, depending only on μ, r, L, S_0, and p, such that whenever $W_{2p}(\mu,\mu')\le r$,

$$W_p^p\big(\mathcal{T}(\mu),\mathcal{T}(\mu')\big)\le C_{\mu,r}W_{2p}^p(\mu,\mu').$$

Equivalently,

$$W_p\big(\mathcal{T}(\mu),\mathcal{T}(\mu')\big)\le C_{\mu,r}^{1/p}W_{2p}(\mu,\mu').$$

Now, given any $\varepsilon>0$, choose

$$\delta:=\min\left\{r,\frac{\varepsilon}{C_{\mu,r}^{1/p}}\right\}.$$

Then, whenever $W_{2p}(\mu,\mu')<\delta$, we have

$$W_p\big(\mathcal{T}(\mu),\mathcal{T}(\mu')\big)<\varepsilon.$$

Thus, $\mathcal{T}$ is continuous at μ from the W_{2p} topology to the W_p topology. Since $\mu\in\mathcal{P}_{2p}(\mathbb{R}^N)$ is arbitrary, the proof is complete.

REFERENCES

[1] A. Sandryhaila and J. Moura, "Big data analysis with signal processing on graphs: Representation and processing of massive data sets with irregular structure," *IEEE Signal Process. Mag.*, vol. 31, no. 5, pp. 80–90, 2014.

[2] D. I. Shuman, S. K. Narang, P. Frossard, A. Ortega, and P. Vandergheynst, "The emerging field of signal processing on graphs: Extending high-dimensional data analysis to networks and other irregular domains," *IEEE Signal Process. Mag.*, vol. 30, no. 3, pp. 83–98, 2013.

[3] A. Ortega, P. Frossard, J. Kovačević, J. Moura, and P. Vandergheynst, "Graph signal processing: Overview, challenges, and applications," *Proc. IEEE*, vol. 106, no. 5, pp. 808–828, 2018.

[4] B. Girault, A. Ortega, and S. S. Narayanan, "Irregularity-aware graph Fourier transforms," *IEEE Trans. Signal Process.*, vol. 66, no. 21, pp. 5746–5761, 2018.

[5] F. Ji and W. P. Tay, "A Hilbert space theory of generalized graph signal processing," *IEEE Trans. Signal Process.*, vol. 67, no. 24, pp. 6188 – 6203, 2019.

[6] X. Jian, F. Ji, and W. P. Tay, "Generalizing graph signal processing: High dimensional spaces, models and structures," *Foundations and Trends® in Signal Processing*, vol. 17, no. 3, pp. 209–290, 2023.

[7] A. Ortega, *Introduction to Graph Signal Processing*. Cambridge University Press, 2022.

[8] H. Huang, N. Sunar, and J. Swaminathan, "Do noisy customer reviews discourage platform sellers? empirical analysis of an online solar marketplace," *SSRN Electronic Journal*, 2020.

[9] F. Ji, X. Jian, W. P. Tay, and M. Yang, "Processing asynchronous time-simplex signals," in *European Signal Processing Conference (EUSIPCO)*, 2025, pp. 2417–2421.
[10] N. Perraudin and P. Vandergheynst, "Stationary signal processing on graphs," *IEEE Trans. Signal Process.*, vol. 65, no. 13, pp. 3462–3477, Jul. 2017.
[11] A. G. Marques, S. Segarra, G. Leus, and A. Ribeiro, "Stationary graph processes and spectral estimation," *IEEE Trans. Signal Process.*, vol. 65, no. 22, pp. 5911–5926, Aug. 2017.
[12] X. Jian, W. P. Tay, and Y. C. Eldar, "Kernel based reconstruction for generalized graph signal processing," *IEEE Transactions on Signal Processing*, pp. 1–15, 2024.
[13] A. Kroizer, T. Routtenberg, and Y. C. Eldar, "Bayesian estimation of graph signals," *IEEE Trans. Signal Process.*, vol. 70, no. 5, pp. 2207–2223, Mar. 2022.
[14] X. Jian and W. P. Tay, "Wide-sense stationarity in generalized graph signal processing," *IEEE Transactions on Signal Processing*, vol. 70, pp. 3414–3428, 2022.
[15] G. Sagi and T. Routtenberg, "MAP estimation of graph signals," *IEEE Transactions on Signal Processing*, pp. 1–16, 2023.
[16] S. Sardellitti, S. Barbarossa, and P. D. Lorenzo, "Graph topology inference based on sparsifying transform learning," *IEEE Trans. Signal Process.*, vol. 67, no. 7, pp. 1712–1727, 2019.
[17] X. Dong, D. Thanou, P. Frossard, and P. Vandergheynst, "Learning laplacian matrix in smooth graph signal representations," *IEEE Trans. Signal Process.*, vol. 64, no. 23, pp. 6160–6173, Dec. 2016.
[18] F. Ji, W. P. Tay, and A. Ortega, "Graph signal processing over a probability space of shift operators," *IEEE Transactions on Signal Processing*, vol. 71, pp. 1159–1174, 2023.
[19] S. Lee, F. Ji, K. Xia, and W. P. Tay, "Graph neural networks with a distribution of parametrized graphs," *Proc. ACM Int. Conf. Machine Learning (ICML)*, 2024.
[20] C. Villani, *Optimal Transport, Old and New*. Springer, 2009.
[21] A. Kolmogorov, *Foundations of the Theory of Probability*. New York: Chelsea., 1956.
[22] R. Durrett, *Probability: Theory and Examples (5th ed.)*. Cambridge University Press, 2019.
[23] W. Rudin, *Real and Complex Analysis*. McGraw-Hill, 1987.
[24] M. Puschel and J. Moura, "Algebraic signal processing theory: Foundation and 1-D time," *IEEE Trans. Signal Process.*, vol. 56, no. 8, pp. 3572–3585, 2008.
[25] F. Ji, S. H. Lee, H. Meng, K. Zhao, J. Yang, and W. P. Tay, "Leveraging label non-uniformity for node classification in graph neural networks," in *Proc. International Conference on Machine Learning*, vol. 202, 2023.
[26] F. Ji, Y. Zhao, S. H. Lee, K. Zhao, W. P. Tay, and J. Yang, "Graph distributional signals for regularization in graph neural networks," *IEEE Trans. Signal Inf. Process. Netw.*, vol. 11, pp. 670–682, 2025.
[27] Y. Zhao, F. Ji, X. Jian, and W. P. Tay, "Graph distribution-valued signals: A wasserstein space perspective," in *Proc. IEEE Int. Conf. Acoust., Speech, Signal Process.*, May 2026.
[28] J. Delon and A. Desolneux, "A wasserstein-type distance in the space of gaussian mixture models," *SIAM Journal on Imaging Sciences*, vol. 13, no. 2, pp. 936–970, 2020.
[29] Y. Chen, T. T. Georgiou, and A. Tannenbaum, "Optimal transport for gaussian mixture models," *IEEE Acess*, vol. 7, pp. 6269–6278, 2018.
[30] A. Sklar, "Fonctions de répartition à n dimensions et leurs marges," *Publ. Inst. Statist. Univ. Paris*, vol. 8, pp. 229–231, 1959.
[31] F. Durante, J. Fernández-Sánchez, and C. Sempi, "A topological proof of sklar's theorem," *Applied Mathematics Letters*, vol. 26, no. 9, pp. 945–948, 2013.
[32] Y. Lecun, L. Bottou, Y. Bengio, and P. Haffner, "Gradient-based learning applied to document recognition," *Proceedings of IEEE*, vol. 86, no. 11, pp. 2278–2324, 1998.
[33] M. Cuturi, "Sinkhorn distances: Lightspeed computation of optimal transport," *Advances in Neural Information Processing Systems*, pp. 2292–2300, 2013.
[34] R. Sinkhorn, "Diagonal equivalence to matrices with prescribed row and column sums," *Proceedings of the American Mathematical Society*, vol. 45, pp. 195–198, 1974.
[35] J. Altschuler, J. Weed, and P. Rigollet, "Near-linear time approximation algorithms for optimal transport via sinkhorn iteration," *Advances in Neural Information Processing Systems*, pp. 1964–1974, 2017.
[36] A. DasGupta, *Asymptotic Theory of Statistics and Probability*. Springer, 2008.
[37] A. Sandryhaila and J. Moura, "Discrete signal processing on graphs: Frequency analysis," *IEEE Trans. Signal Process*, vol. 62, no. 12, pp. 3042–3054, 2014.
[38] ——, "Discrete signal processing on graphs," *IEEE Trans. Signal Process.*, vol. 61, no. 7, pp. 1644–1656, 2013.
[39] D. Ramírez, A. G. Marques, and S. Segarra, "Graph-signal reconstruction and blind deconvolution for structured inputs," *Signal Processing*, vol. 188, p. 108180, 2021.
[40] E. Isufi, F. Gama, D. I. Shuman, and S. Segarra, "Graph filters for signal processing and machine learning on graphs," *IEEE Transactions on Signal Processing*, vol. 72, pp. 4745–4761, 2024.
[41] S. Kwak, N. Geroliminis, and P. Frossard, "Traffic signal prediction on transportation networks using spatio-temporal correlations on graphs," *IEEE Transactions on Signal and Information Processing over Networks*, vol. 7, pp. 648–660, 2021.
[42] NIHR Evidence, "Epilepsy: what are the chances of having a second seizure?" 2023, accessed: 2026-03-08.
[43] H. E. Egilmez and A. Ortega, "Spectral anomaly detection using graph-based filtering for wireless sensor networks," 2014, pp. 1085–1089.
[44] S. Chen, A. Sandryhaila, J. M. F. Moura, and J. Kovačević, "Signal recovery on graphs: Variation minimization," *IEEE Trans. Signal Process.*, vol. 63, pp. 4609–4624, Sep. 2015.
[45] J. An and S. Cho, "Variational autoencoder based anomaly detection using reconstruction probability," *Special lecture on IE*, vol. 2, no. 1, pp. 1–18, 2015.
[46] D. P. Kingma and M. Welling, "Auto-encoding variational bayes," *arXiv preprint arXiv:1312.6114*, 2013.
[47] P. Billingsley, *Convergence of Probability Measures*, 2nd ed. New York, NY, USA: Wiley, 1999.